Fabrication of a microporous PDMS membrane for an Organ-on-Chip device

Jose Manuel Rosas Escobar

Master of Science Thesis

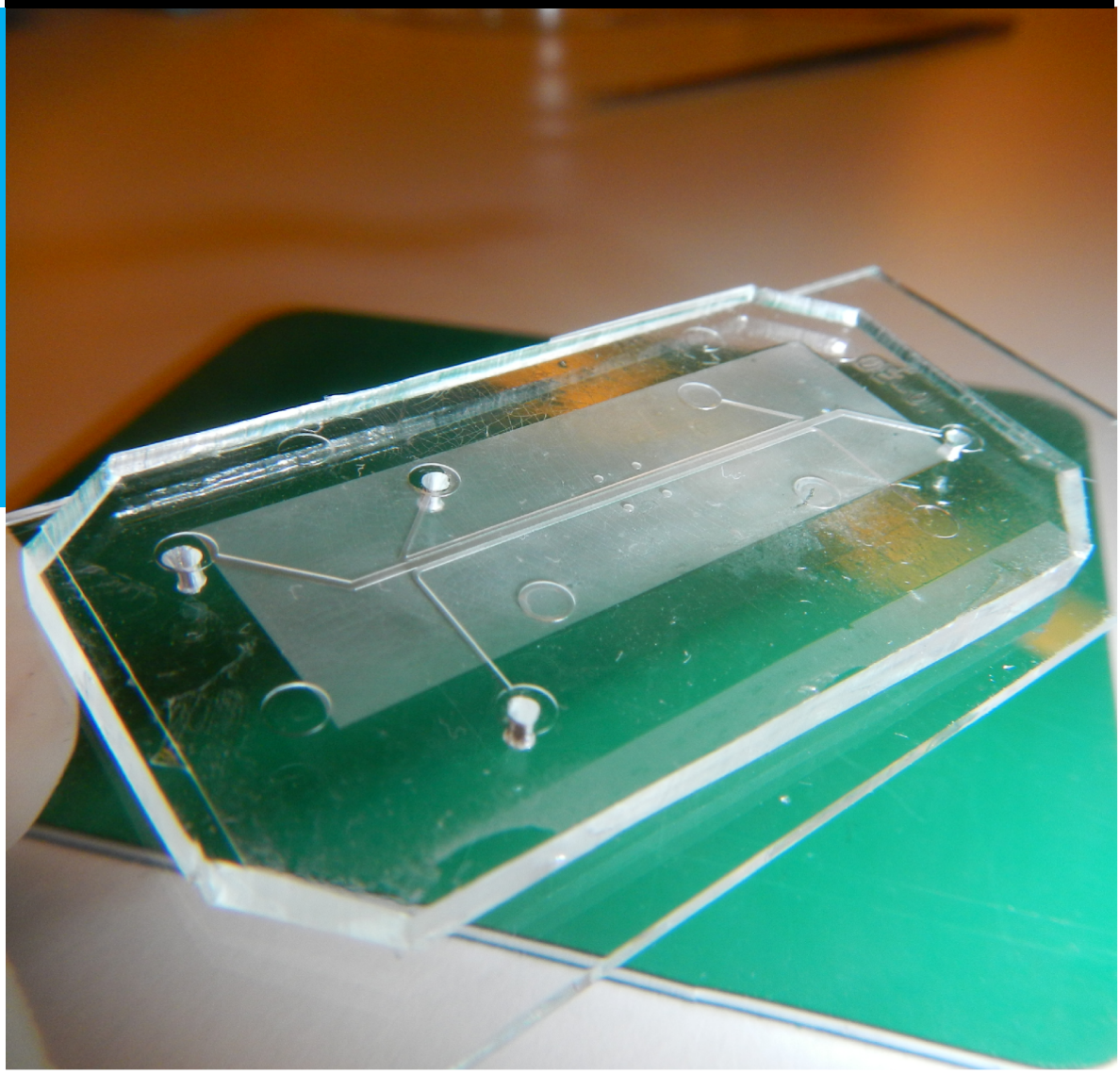

TU Delft Delft University of Technology

Delft Institute for Microsystems and Nanoelectronics

Fabrication of a microporous PDMS membrane for an Organ-on-Chip device

Master of Science Thesis

For the degree of Master of Science in Biomedical Engineering at Delft University of Technology

Jose Manuel Rosas Escobar

November 7, 2014

Faculty of Mechanical, Maritime and Materials Engineering (3mE) · Delft University of Technology

The work in this thesis was supported by TU Delft, TU Eindhoven and Philips Research. Their cooperation is hereby gratefully acknowledged.

Delft University of Technology
Department of
Delft Institute for Microsystems and Nanoelectronics(dimes)

The undersigned hereby certify that they have read and recommend to the Faculty of Mechanical, Maritime and Materials Engineering (3mE) for acceptance a thesis entitled

Fabrication of a microporous PDMS membrane for an Organ-on-Chip device

by

Jose Manuel Rosas Escobar

in partial fulfillment of the requirements for the degree of

Master of Science Biomedical Engineering

Dated: November 7, 2014

Supervisor(s):

prof.dr.ir. Ronald Dekker

prof.dr.ir. J.M.J den Toonder

dr. Anja van de Stolpe

Reader(s):

dr. R. Ishihara

prof.dr. P.J. French

Abstract

Organs on chips are a novel set of devices whose aim is to mimic cellular in-vivo conditions of the human physiology within a microchip. The need of reliable disease models, particularly for the development of pharmaceutical drugs, has drawn increased attention as the current widespread models; static cell cultures and animal tests, have proven poor predictability, are costly and are increasingly ethically problematic. By providing physiologically relevant bio-chemical, mechanical and other relevant cues to the cells cultured, these in-vitro 'organs' develop similar characteristics to those observed in their in-vivo counterparts. To achieve this, these chips are carefully designed and fabricated with various micro-fabrication technologies, in particular soft-lithography, due to its extensive use for microfluidic devices and materials' proven biological compatibility. However, standard soft-lithography presents major drawbacks as a platform for mass-scale fabrication of complex devices, in particular the extensive use of manual processing which makes it un-reliable and promotes break of thin substrates. At the Eindhoven University of Technology, an Organ-on-chip is being developed to study cancer cell dissemination; cancer metastasis, and several design features have been identified. In particular, the need of a thin micro-porous substrate that allows multiple-cells to be cultured in close contact, bio-chemical and mechanical stimuli, and migration of cells through this layer. Though several soft-lithographic techniques have been reported for the fabrication of similar thin porous films, the manual handling problem has been assessed to be the major technical bottle-neck.

In this thesis, a fabrication method based on soft-lithography was designed to make thin micro-porous elastomeric membranes and a brief evaluation of their characteristics to be used for a Cancer-on-Chip was done. By integrating a selective sacrificial layer approach in the soft-lithographic molding process of the membrane, we have addressed the manual handling problem. This enabled us to fabricate large area thin PDMS membranes with micro-pores of 7 μm to 10 μm diameter. The membranes were successfully integrated in micro-fluidic devices and tested for reliability, robustness and porosity by mass transport experiments. Validation for its compatibility for cancer cell culturing was done by seeding breast cancer cells and observing their adhesion on and migration through the membrane.

Table of Contents

List of Figures

List of Tables

Preface & Acknowledgement

This thesis is the final requirement to obtain the Master's degree in Biomedical Engineering at Delft University of Technology. The project was conducted in the Research Group Microsystems in the Department of Mechanical Engineering at the Eindhoven University of Technology. This project has been a collaboration between TU Delft, TU Eindhoven and Philips Research in Eindhoven, The Netherlands, to set the grounds for an Organ-on-chip microfluidic device to study cancer metastasis. Though, originally the aim was to replicate a reported manufacturing process to fabricate a porous membrane and also design a chip to stimulate cancer cells in which to integrate the membrane, the fabrication process pursued provided inconsistent results and therefore we set to develop a new method to address the previously observed problems for fabricating a porous membrane. This work, together with the literature survey generated during this time, therefore, set the physiological background, design constraints, techniques and technology considerations to create a Cancer-on-Chip device. With the technique described in this thesis we hope to empower research groups interested in the development of Organs-on-Chips and at the same time to bring our own goal of a Cancer-on-Chip nearer to reality.

I would like to thank my supervisor Prof. Jaap den Toonder at TU Eindhoven, for his guidance, example and for trusting in me to contribute in his vision, a Cancer-on-Chip. I am also thankful with Dr. Anja van de Stolpe at Philips Research for her assistance and incredible enthusiasm to discover the mysteries cells carry with them. Special thanks to Regina Luttge, whose insights and words resonate within me as a reminder to focus in order to achieve the proposed goal, this is a lesson I cherish truly. And mostly, I am greatly thankful to Prof. Ronald Dekker at TU Delft, for his transparency, constant motivation and caring. Special thanks to Hossein Eslami; for all his input, his smile and friendship during the entirety of the project, to Tom van Gijsel; for his pro-activity, his belief in what we do, and for his self-less help with the cell experiments, to Angel Savov; for his friendship and all his help during the project, without him the collaboration with Philips Research would have not occurred, to Shivani Joshi; for her help in the first part of my project and for her friendship during the completeness of it, and to Jasper Beerens; with whom I had the pleasure to share this adventure and to whom I wish the best.

Delft, University of Technology — MSc. Biomedical Engineering

Master of Science Thesis — Jose Manuel Rosas Escobar

Dedicado a la memoria de mi hermana

y a quienes me han amado siempre, incondicionalmente, inconmensurablemente, mi padre y madre.

Chapter 1

Introduction

Traditional in-vitro cell cultures and animal models have been throughly used to study cell function, diseases and are used as disease models to assess drug efficacy. Unfortunately, every time more it has been shown that their predictive effectiveness is limited and that these heavily fail to provide a correct assessment of possible side-effects [1]. On one hand, typical in-vitro cell cultures consisting of static cell and medium assays used are rough simplifications of the in-vivo physiology. Furthermore, cells seeded in these assay do not behave nor have the same characteristics as in-vivo. Evidence points that the lack of providing cells with physiological relevant cues and an appropriate micro-environment; such as dynamic bio-chemical and mechanical stimuli, is associated to these differences [2]. On the other hand, animal models are able to reproduce some key physiological features which enhance their prediction of complex and systematic system behavior. Nevertheless, crucial differences between animal to human physiology make this still fail to account for possible fatal variations associated to side and long-term effects in humans. Together with increasingly ethical concerns [3] and their high cost [1, 2], while offering little controllability and methods to assess progression, has spawn a fervent need to consider alternative disease models.

1-1 Organ-on-Chip

Organ-on-Chip (OoC) is a novel cell culture platform that intends to overcome the limitations of the traditional methods by mimicking essential human organs and tissues by seeding cells in specially designed devices that simulate particular micro-environments in the human body. Inside these, individual or multiple types of human cells can be cultured and stimulated with well controlled biochemical and mechanical cues, thus resembling in-vivo micro-environment conditions [4]. Providing these cues to cells has been observed to help them organize and respond similarly as they would normally in-vivo, and in this way healthy and disease scenarios and functions of tissues can be studied and used to test the effects of potential therapeutic drugs.

Microfluidic chips; most commonly made in an elastic, transparent and inert silicone elastomer called polydimethylsiloxane (PDMS), have been proven particularly suitable to host

cell cultures while maintaining fluid bio-chemical environments that can be fashioned in similar size-ranges as in-vivo micro-environments. PDMS microfluidic devices, commonly made by a molding technique called soft-lithography; in which the liquid pre-polymer is poured onto a negative mold, cured and then peeled, have the advantage of being fabricated in a straightforward manner, relatively cheap and need of little specialized equipment in an out-of-cleanroom environment.

The Lung-on-chip; developed at Wyss Institute at Harvard [2], is an example of a device fully made in PDMS by standard soft-lithographic techniques. This device comprises fluid and pneumatic channels for bio-chemical and mechanical stimulation while allowing co-culture of lung and endothelial cells in close contact. A porous PDMS membrane separating two fluid channels is used as a compartmentalizing substrate for the co-culture, on one side the lung cells are seeded and in the other the endothelial cells. This membrane has holes that allow direct contact of cells but also possible diffusion of species from one channel to the other. Additionally the high compliance of the substrate allows it to be cyclically stretched and therefore provide mechanical stimulation to the attached cells. On the other hand, other organs-on-chips require specialized micro-fabrication techniques to have the features needed for their intended functionality. The Cytostretch (Heart-on-chip) developed in collaboration between TU Delft and Philips Research [5], is an example of such a device. This device is an stretchable micro-electrode-array (SMEA) in which electrode tracks are embedded in a PDMS film. Cardiac cells seeded on the film are stimulated via pneumatic inflation of the film while conducting electrical characterization of cell activity. Though different designs and functionalities are needed for each 'organ' chip, most have in common the need of a suitable substrate to allow bio-chemical stimulation and direct communication between compartmentalized cell types which make up for the basic functional units of organs.

1-1-1 Cancer-on-Chip

Metastasis, which is the invasion of cancerigenous cells from a primary solid tumor to secondary sites in distant and near organs in the body is the leading; 90% [6], cause of death from cancer [7]. A solid tumor in itself is a complex and heterogeneous micro-environment hosting tumor cells between others. Much like an organ, this micro-environment provides tumor cells with biochemical and mechanical stimulation which is hypothesized to promote tumor cells to become cancerous and furthermore activate cancer metastasis [8]. Cancer progression towards metastasis is a complex stepwise interplay of many factors within and out of the tumor such as the invasion of different types of cells (e.g. various kinds of white blood cells) and permeation of soluble factors (e.g. oxygen) into the tumor mass via the permeating blood vessels. And though many discrete cellular processes have been identified in metastasis progression, it is widely unknown which specific factors and conditions trigger it [9]. The development of an Organ-on-Chip model is therefore of particular interest for its capability to replicate the tumor micro-environment and study the activation factors in the micro-environment that lead towards metastasis.

Such a device, a Cancer-on-Chip, is in development at the Eindhoven University of Technology (TU/e) in the form of a multi-chamber microfluidic device. The conceptualized device, depicted in Figure 1-1a, enables the study of metastasis by recreating a primary tumor site and the process of cancer cells migrating from here through the blood stream, invading an

organ and creating a secondary tumor, i.e. a metastatic site. Both the primary tumor and the metastatic site are conceived as a co-culture of tumor or organ cells and endothelial cells (representing the blood-vessel lining) separated by a porous membrane. In the primary tumor site, where transition towards cancer and invasion to the blood-vessel occurs, the porous membrane is the most important feature of the device (Figure 1-1b). While it serves as a substrate for 3D culture of cancer cells and a 2D cell mono-layer of endothelial cells, it also allows bio-chemical stimulation of the cancer cells; by allowing species transport through its pores, and possible relevant mechanical stimulation; for example by applying cyclic stretch of the cells attached, to trigger metastatic progression.

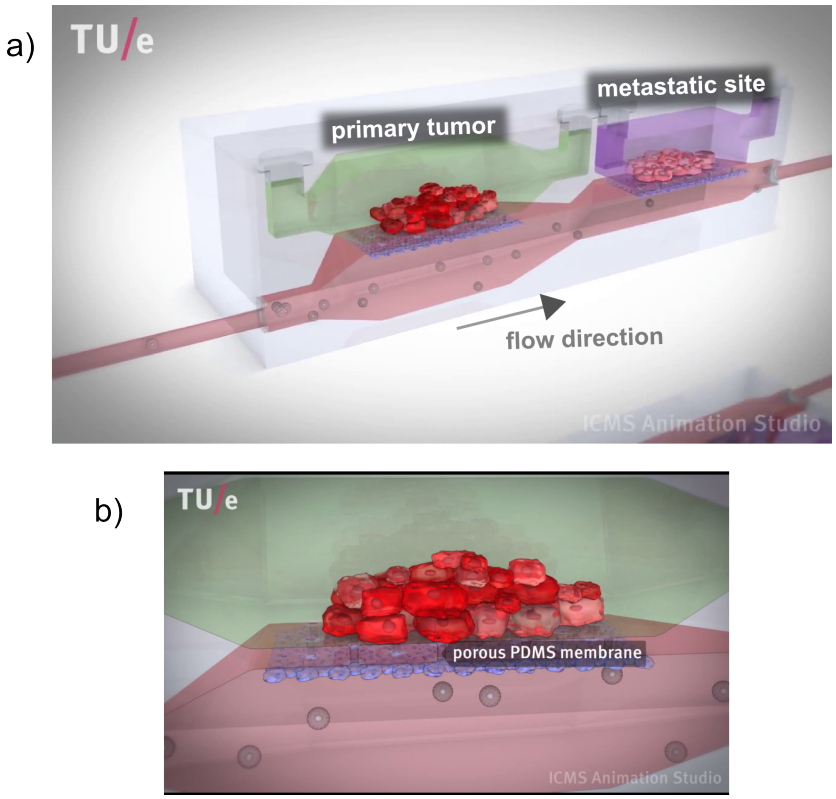

Figure 1-1: *(a) Conceptualization of a Cancer-on-Chip microfluidic device to study cancer metastasis. (b) Co-culture of 3D tumor cells and a 2D endothelial cell monolayer separated by a porous membrane. The design of the device is able to exert fluid and mechanical stimulation to promote migration of the tumor cells into the lower blood-stream channel. A porous PDMS membrane is conceived as a suitable substrate to provide the necessary stimulation while allowing cell compartmentalization, communication and migration. Images from 'Cancer metastasis on a chip', associated literature [3].*

1-2 Scope and organization of this thesis

The goal of this thesis project was to fabricate and characterize a thin microporous PDMS membrane to act as a suitable substrate for the proposed Cancer-on-Chip device.

The particular objectives and guidelines to reach the project goal can be summarized as:

1. Develop a fabrication process that is repeatable and accessible with standard soft-lithographic techniques.
2. Assess the membranes' integrability into a micro-fluidic device and test its characteristics to act as a permeable barrier to fluid flow.
3. Assess the membranes' suitability as a substrate for a co-culture of cancer cells and a second cell type to test adhesion and migratory ability of cancer cells through it.

1-2-1 Organization of this thesis

The main chapters of this thesis; chapter II Background, chapter III Experimental, chapter IV Results and Discussion, and chapter V Conclusion, have been organized and are presented in the form of a publishable paper. We have decided to present the work and results of the developed methodology in this form as we believe that this technique is novel from what has been previously presented in the literature, and since adaptations or direct use of it could represent a technical contribution for the development of the field of soft-lithographic micro-fabrication.

In chapter II, an overview of micro-fabrication techniques and technologies for the fabrication of porous elastomeric membranes is given. The main trends are discussed and also the disadvantages of using standard soft-lithography.

In chapter III, the experimental methodology developed for fabrication of membranes is explained. Also, the micro-fluidic setup used for its characterization is described as well as the set in which the membranes were incorporated for relevant cell experiments.

Chapter IV presents the results obtained from analyzing the fabricated membranes by SEM imaging, fluidic characterization and cell experiments. Additionally, a discussion on the observed results and their relationship with the manufacturing process is given.

The final chapter of this paper, chapter V, gives a conclusion of the developed process, the membranes produced with it, and the characterization methodologies used for analyzing the membranes' properties.

To complement this work, a set of appendices is given to cover in detail: the fabrication procedure used (Appendix A), a troubleshooting section of the fabrication procedure (Appendix B), a detailed explanation of the analysis procedure for the SEM and fluid characterization results (Appendices C & D), a detailed section of the physiological background on cancer and practical considerations for cell culturing (Appendix E) that led to the cell characterization experiments (Appendix F).

A novel fabrication method for thin microporous elastomeric membranes introducing selective sacrificial layers in soft lithography

Jose M. Rosas,[ab] Tom van Gijsel,[c] Anja van de Stolpe,[c] Ronald Dekker,[bc] and Jaap M.J. den Toonder,[ad*]

—The integration of thin (~10μm) micro-porous membranes in microfluidic devices has been of recent interest since these are central for use in mass transport applications and more recently in biological assays. One particular example are Organ-on-chip (OoC) platforms, in which membranes serve as supports for cell culture while allowing for complex mechanical and bio-chemical stimuli to be applied. Polydimethylsiloxane (PDMS) membranes are of particular interest for their advantageous mechanical, chemical and optical properties. Reported micro-fabrication approaches to make thin porous PDMS membranes range from expensive methods that involve a combination of dry etching and spin-coating and that require an expensive infrastructure, to soft lithography approaches using spin-coating and cast-molding that are less costly and are therefore more widely accessible to researchers. The latter methods, however, generally show poor reproducibility that can be mostly attributed to manual handling procedures inherent to soft-lithography. In this paper we describe a straightforward and repeatable method to mold and transfer thin micro-porous PDMS membranes by extending conventional soft-lithographic techniques. Two specific sacrificial layers are introduced that can be selectively removed; one on a mold with SU-8 micro-features that eventually define the pores of the membrane, and another on a thick PDMS slab acting as a carrier substrate. A PDMS film with through pores is made by pressing uncured PDMS in between. Once the thin film is cured, it can first be released from the mold and then from the carrier substrate by subsequent immersion in acetone and water. This method for de-molding and transfer decreases manual handling, thus avoids breaking, tearing and self-folding of the membrane; additionally, it circumvents the use of expensive equipment and toxic materials such as solvents that could compromise their use in bio-assays. To test the mechanical robustness, sealing and porosity of the membranes made by this method we have integrated these in a criss-cross microfluidic device and evaluated forced advective flow through the membrane. Additionally, to test bio-compatibility we have integrated our membrane in a chemotactic cell assay to evaluate compatibility with cell culture as well as the migration of cells through the pores.

II. BACKGROUND

MEMBRANES are used for a variety of purposes ranging from particle separators to flexible substrates for cell assays or scaffolds [1]. Though many papers have concentrated on the use of membranes for microfluidic devices, relatively little diverse applications have been explored, probably because of either, processing limitations of commercially available membranes made of thermoplastics or because of the need to use state-of-the-art processes and expensive equipment to fabricate membranes of other materials.

Two major approaches are normally followed for integrating membranes into microfluidic devices, namely one in which (ready-made) membranes are integrated into the device, and the other in which the membrane is fabricated together with the device [1]. The first, integration of commercially available polycarbonate (PC) and polyethylene terephthalate (PET) track etched membranes has been widely applied for use in biological assays, though it is often reported that the integration of these membranes in a micro-fluidic device is difficult and results in problems such as leakage [1] and poor bonding [2]. Moreover the PC and PET properties sometimes are limiting, as their translucency limits optical microscopy, and their relatively high elastic modulus (~GPa) limits their use as a mechanical actuator [1]. To alleviate these disadvantages, there has been a recent interest in fabricating and integrating thin microporous films of polydimethylsiloxane (PDMS) in microfluidic devices. PDMS is a silicone elastomer which is highly compliant (with an elastic modulus of 1-3 MPa [3]), optically transparent (in the wavelength range 240−1100*nm* [4]), and it can be reversibly or irreversibly bonded to silicon, glass, or PDMS hence avoiding overall leakage when integrated in microfluidic devices [1]. Furthermore, PDMS is attractive for its compatibility with biological materials, for example in cell culture assays, due to properties such biological inertness and high oxygen permeability. Microporous PDMS membranes can be used as substrates for cell assays in novel bio platforms as Organ-

This work was supported in part by the Mexican National Council of Science and Technology (CONACYT).

[a] Department of Mechanical Engineering, Eindhoven University of Technology, Eindhoven, The Netherlands. (e-mail: jmrosasescobar@gmail.com).

[b] Delft Institute for Microsystems and Nanoelectronics, Delft University of Technology, Delft, The Netherlands.

[c] Philips Research, Eindhoven, The Netherlands.

[d] Institute for Complex Molecular Systems, Eindhoven University of Technology, Eindhoven, The Netherlands.

**Correspondence to: Prof. Jaap den Toonder (TU/e Department of Mechanical Engineering, Eindhoven, Postbus 513, 5600 MB; Tel.: +31 (0)40247-57-06;E-mail:J.M.J.d.Toonder@tue.nl)*

‡ Electronic supplementary information (ESI) available: Detailed fabrication process, fabrication troubleshooting and characterization analysis and methodology.

on-a-chip (OoC) where they can act as interfaces between different cells in co-culture, while still allowing for (cell) communication and transport of matter through the membrane [5,6].

PDMS membrane fabrication has been reported in the literature by two different fabrication approaches. One approach makes use of standard micro-fabrication techniques such as direct etching, and the other uses soft-lithographic techniques relying on molding. While membrane fabrication by anisotropic dry etching (CF4:O2 or SF6:O2 mixtures with etch rates of max $\sim 0.8\mu m \cdot min^{-1}$) has been previously shown [7, 8], these processes are technology restrictive as they require expensive equipment as well as laborious process tweaking. Alternatively, thin porous membranes have been realized by spin coating or stamping PDMS films over a substrate with microscopic features defining the pores and subsequent curing and de-molding. For spin-coating, PDMS is commonly diluted with a suitable solvent, e.g. hexane or toluene, to decrease its viscosity and therefore achieve thin layers, typically thinner than 5µm [9, 10, 11]. However, three major issues have been observed with the spin-coating approach. First, hydrodynamically induced defects can be introduced in the thin film due to interaction between the wetting PDMS layer and the geometrical features on the substrate [12]. Secondly, when spin-coated, PDMS tends to create an ultra-thin layer on top of the features which eventually results in closed pores. This may be avoided by using features that are substantially higher than the spincoated PDMS film, but this increases the risk of hydrodynamically induced defects and also breaking of the features [10]. Thirdly, due to poor mechanical properties of the thin membrane it is often difficult to de-mold it without breaking or tearing. To avoid this, the use of anti-stiction coatings, supporting rims and coating with mechanically tougher layers for handling has been advised [7,10,11,12]. A method based on capillary filling rather than spincoating, in combination with a silane surface modification, has recently been reported as a simple way to make porous PDMS membranes [13], although the technique has been demonstrated only with thicker films (~40µm) and with few features. Recently, a replica molding process [5,6] has been shown to create a highly porous (9%) thin (~10µm) PDMS membrane by first spin coating a uniform PDMS layer and subsequently stamping it onto a silanized silicon pillar mold while curing. Though this process has been successful at making membranes, two major problems have been observed, namely tearing or breaking of the membrane when de-molding due to manual handling, and unwanted adhesion between the mold and membrane, and blockage of membrane pores.

To alleviate demolding problems for thin films, several sacrificial layer approaches have been recently reported for lift-off and transfer of patterned SU8 layers [14,15,16,17]. Photoresist is commonly used as a photo-patternable mask layer for microelectronic technology and more recently its use has been extended as a sacrificial layer and as an aid for lift-off processes of SU-8 microstructures. Recently, photoresist has also been proven to be a useful soluble masking layer for PDMS dry etching by reducing its poor adhesion to PDMS by applying an O_2 plasma treatment [7]. Other sacrificial layers have been recently explored, in particular polyacrylamide (PAA), Dextran and polyvinyl-alcohol (PVA) [16,17], which are soluble in water. These materials possess also processing advantages as they can be spin coated, and can be released in DI water at low temperatures; this makes them attractive for combining with sensitive materials and for processing devices for biological applications.

In this paper, we present an easy-to-implement method to mold and transfer well-defined thin microporous PDMS membranes using selective sacrificial layers that can be spin-coated. Our approach reduces failure by tearing or breaking since manual handling is minimized. No hazardous etching chemicals are necessary since only acetone and water are used for the release. Our molding and transfer technique enables high resolution of through-features ($\gtrsim$ 7µm) in thin (~10 µm) PDMS layers while allowing large area defect free fabrication and transfer to PDMS-based microfluidic devices (~3 cm^2). As proof of their general application we have integrated the membranes in a criss-cross microfluidic device to characterize transport of material through the membranes and we have assessed their bio-compatibility in a cell-migration setup.

III. EXPERIMENTAL SECTION

A. *Membrane Molding and Transfer*

The fabrication process for molding and release of PDMS membranes is illustrated in Fig. 3-1. Pentagonal pillar features (10 µm diameter, 30 µm pitch) are patterned in a standard photolithographic process. First, an ~10 um layer of SU-8 2015 (SU-8 2000 from MicroChem Corp.) is spincoated onto a clean silicon substrate (30 sec, 2700 rpm) and patterned by exposure to UV (35 sec, $11.4mW \cdot cm^{-2}$) through a chrome-on-glass mask (Techno-Mask, Eindhoven, The Netherlands). Development of the features is performed by submersing in SU-8 developer (mr-Dev600, Micro-resist Technology, duration > 10min) with mild stirring. A final hard bake (20 min at 200 ^{0}C with ramp-up and ramp-down to RT) is applied to improve mechanical properties of the mold thus obtained. Next a positive photoresist (Microposit S1813 G2 from Shipley, Marlborough, USA.) layer (~**1** µm) is spincoated (30 sec, 4000 rpm) and baked (5 min at 110 ^{0} C) on the SU-8 mold to serve as an anti-adhesion coating for PDMS and a interface that is soluble by acetone rinsing. Additionally, this resist is suitable to be spincoated in thicknesses between approx. 2 µm down to submicron (~5 µm) thus maintaining the pillar profile dimensions.

In parallel, a ~4 mm thick poly (dimethylsiloxane) (PDMS) (Sylgard 184 from Dow Corning Corp, Midland, MI.) is prepared by pouring a 15:1 (base-to-curing agent) degassed mixture on a clean silicon wafer and curing it overnight at room temperature on a leveled surface. The slab is cut (2.5 cm x 4 cm and corners removed at 45^0 angles) and attached to a clean microscope glass slide. The PDMS slab surface is then treated with air plasma (20 W for 35 sec) to make the surface temporarily hydrophilic and immediately a 20% (w/v) dextran (Dextran 70, Sigma Aldrich, The Netherlands) and DI water solution is dispensed onto the surface and spin coated (30 sec, 4000 rpm) to achieve a uniform thin layer (of ~1 µm thickness). The coated layer on the slab is dried (~1 hr at 80 ^{0}C) by placing the slab inside a double petri dish covered with absorbent non-fibrous tissue on a hot plate and then left to cool down to room temperature (~1 hr ramp down) before storing it in a clean petri dish for further use. The dextran coated surface should not be touched or disturbed during its processing or handling as this might result in defects in the final membrane.

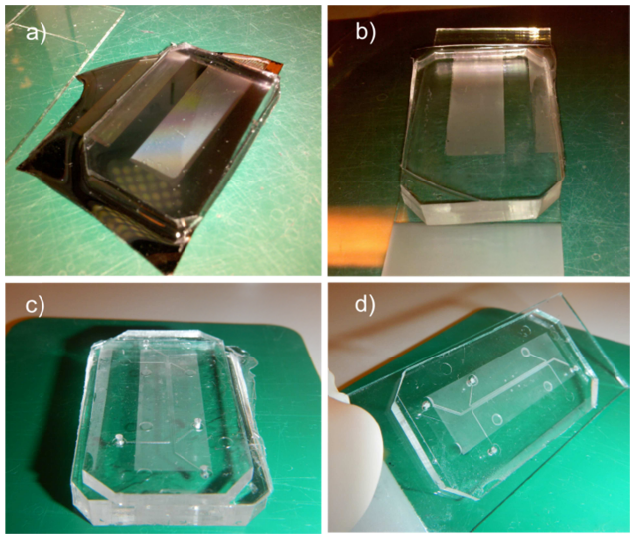

Fig. 3-2 (a) The membrane is molded between the coated SU-8 mold and a thick PDMS coated slab. The slab remains adhered until released (step f in Fig.3-1). (b) Membrane adhered to the dextran layer on the PDMS slab carrier after release from mold by acetone bath (step g-h in Fig. 3-1). (c) The membrane is irreversibly bonded to a secondary microfluidic chip by plasma activation and subsequent incubation overnight at 65 ^{0}C (step i in Fig. 3-1). (d) Final microfluidic chip with a 1 cm x 3 cm porous membrane after release by immersion in warm water bath (step j in Fig. 3-1).

A 10:1 PDMS mixture is degassed and poured on the Microposit-coated SU-8 mold; a small amount of the mixture should be dispensed next to the features and left to flow until completely covering the pillar features, to avoid air bubble trapping. Once the molding features are completely covered with a thin uncured PDMS layer, the dextran-coated PDMS slab is gently brought onto conformal

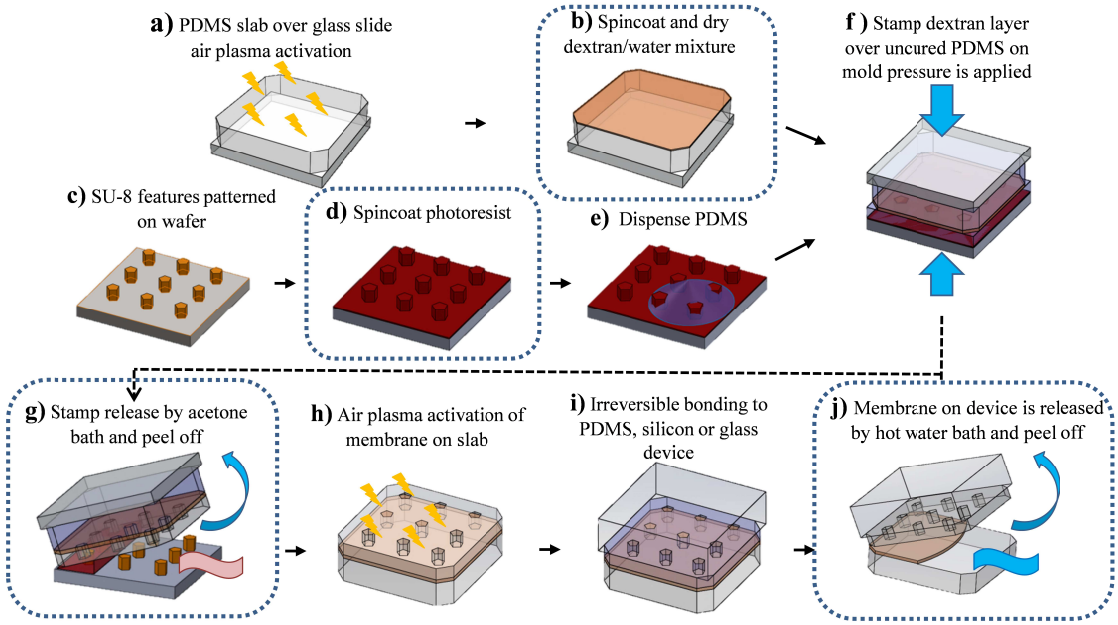

Fig. 3-1 Schematic of soft-lithographic fabrication of a micro-porous PDMS membrane by cast molding and sacrificial layer etching.

contact with the PDMS covered mold and gently released on the mold by tilting, with the dextran surface facing the uncured PDMS mixture. Handling the slab by the glass slide prevents disruption of the dextran layer. Once the slab covers the uncured PDMS, a uniform constant clamping force (~5-10 kg) is gently applied while securing it in place to avoid sliding, and the sandwich is left to cure overnight at room temperature. Two office clamps (32mm, M.N. 296875. Five Star, Acco Brands) provide the clamping force and scotch-tape is applied to keep the mold and glass-slide in position. A final baking step (~1 hr at 75 ^{0}C) is used to ensure complete curing of the membrane before releasing the pressure between mold and slab by carefully removing the clamps and cutting off any excess PDMS.

Removing the microscope glass slide from the thick PDMS slab is done mechanically by inserting and using the tip of fine tweezers or a scalpel as a wedge. De-bonding begins at the corners and a drop of ethanol can be placed at the interface to help the release, though this must be dried before further processing. Fig. 3-2a shows the result. The next step is the release of the slab from the mold by dissolving the sacrificial photoresist layer. First, by using a scalpel, any excess PDMS is cut by making an incision around the perimeter of the bonded PDMS slab to ensure wetting of the Microposit sacrificial layer. The slab is corner can be de-bonded by using the scalpel as a wedge and by placing the mold in an acetone bath (~1 min). Wetting and dissolution of the Microposit layer can be assessed visually during de-molding. A final rinse with acetone ensures a clean and clear PDMS membrane surface. Completion of this step results in a 10 µm thick micro-porous PDMS membrane adhered to the thick PDMS slab by a water-soluble dextran layer (Fig. 3-2b).

The membrane is transferred to a device (e.g. a PDMS microfluidic device) by treating both the slab and the microfluidic device with air plasma (20 W for 35 sec) and then bringing both in conformal contact. An incubation step of ≳ 6 h at 65 ^{0}C is needed to achieve irreversible bonding, after which the device is cooled down in approximately 15 min to room temperature (Fig. 3-2c). The final step is the release of the PDMS slab by dissolving the sacrificial dextran layer. To start this, drops of DI water are placed at the interface between the PDMS slab and the membrane while the corners and surrounding of the interface are slightly lifted by a scalpel to promote water infiltration. For complete release and transfer of the membrane, the set is immersed in a warm water bath (~80-90 ^{0}C) for 1 to5 hrs. or until full release occurs automatically. The release time depends on the dimensions and specific geometry of the device. The final result is shown in Fig. 3-2d

B. Microfluidic characterization setup

Membranes (10 µm thick with 10 µm pores) were bonded to a criss-cross PDMS microfluidic device to evaluate bonding conformity, leakage and porosity. The setup is shown in Fig. 3-3b. The device consists of two PDMS microfluidic channels (~100 µm height and 500 µm width), oriented at an angle of 90^0 with respect to each other, and separated by a membrane section of 1cm x 1cm (Fig. 3-3a). The channels were made by standard soft-lithography from patterning SU8-2050 with an acetate mask and casting 10:1 PDMS on the positive relief. Two 1.2 mm access holes were punched through the cured PDMS substrates and connected to beveled syringe tips and tubing. Two flows (Q_1 & Q_2) are applied to the two input channels by two syringe-pumps (NE-1010- Syringe Pump, ProSense B.V., The Netherlands). In one inlet (flow rate Q_1) a water solution with a constant concentration of black dye (Brilliant Black BN, Dye content 60%, Sigma-Aldrich Chemie BV, The Netherlands) was applied, while in the other (flow rate Q_2) plain DI water was

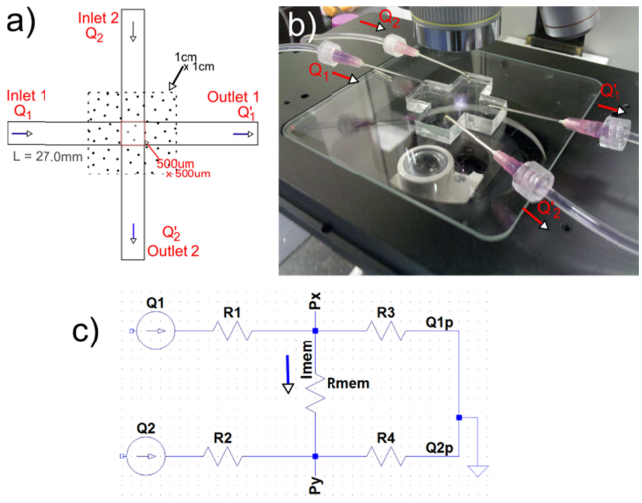

Fig. 3-3 (a) Schematic of the microfluidic characterization setup. Three flow rates were used during the experiment, while $Q_1$was maintained at 10 $\mu l \cdot min^{-1}$, $Q_2$was varied between 10, 7.5 *and* 5 $\mu l \cdot min^{-1}$ to match the proportions discussed ($Q_2 = Q_1, Q_2 = \frac{3}{4}Q_1$ & $Q_2 = 2Q_1$). (b) Fluidic setup used to test porosity. Blunt needles (1 1/2", Terumo Corporation, Japan) connect the device to the inlet and outlet tubing (ACF0002, 1/8", E-3603, Tygon S3, France) via Luer fittings. The inlet tubing pair is of the same length but different from the matching outlet tubing, therefore ensuring R_1=R_2 and R_3=R_4 in the equivalent circuit. Fluid flow in the device and through the membrane, visibility aided by dye content of Q_1 , was assessed during the experiments with bright field miscopy (Leica DM4000 M) and a CCD camera (Leica DFC425 C , Leica Microsystems, Wetzlar, Germany) . (c) Schematic of the electrical circuit model of the microfluidic device. Inlet flows (Q_1 & Q_2) are set represented by current sources. The channel resistances of inlets (R1 & R2) and out lets (R3 & R4) are matched and calculated only for channel section of the device. The resistance of the membrane (R_{mem}) is modelled as N individual pore resistances in parallel. Any compliant (capacitive) effects of the system due to tubing or bending of the membrane have been neglected for simplicity and steady state flow conditions. The outlet channels are connected to ground, which is taken as atmospheric pressure at room temperature.

flown. If the flow rates are equal, i.e. Q_1=Q_2, the transport of the dye through the membrane from one channel to the other is determined by diffusion. If the flow rates differ, a pressure difference over the membrane results in a forced advective flow through the membrane (in our experiments, $Q_2 = \frac{3}{4}Q_1$ & $Q_2 = 2Q_1$). The outlet flows (Q'$_1$ & Q'$_2$) were collected on each outlet port for the duration of the experiment and by quantifying the mass of the volume collected (CPA324S-0CE, Sartorius AG, Germany) the net flow through the membrane was assessed.

The quantified membrane net flow can be correlated to the membrane porosity by comparing the measurements to

predicted outlet flows from an electrical analogue model of the device built in LTspice IV (Linear Technology Corporation, USA), see Fig 3-3c. The model includes the hydraulic resistance of both inlet and outlet rectangular channels $R_{channel} = \frac{12\mu L}{w \cdot h^3}$ as resistors in series and the membrane resistance $R_{membrane} = \frac{1}{N} \cdot (\frac{8\mu t}{\pi \cdot r^4})$, as N resistors in parallel representing the pores present in the membrane [18, 19]. In $R_{channel}$, the channel length is L (13.5 mm), and w and h are the channel width and height respectively. In $R_{membrane}$, N is the number of pores present in the criss-cross section. The fabricated pore density (i.e.~$1111 \frac{pores}{mm^2}$) relates to the size and pitch of the pore distribution thus ideally N is given, t (~10 µm) is the membrane thickness and r (~5 µm) is the pore radius. In practice, the open pore content N varies to the ideal henceforth changing the membrane resistance. The flows (Q'_1 & Q'_2) at the outlets, therefore, are uniquely characterized by a variation of the number of open pores N present in the membrane and the established inlet flows (Q_1 & Q_2).

C. Cell migration setup

To assess biocompatibility and porosity, membranes were incorporated into a static migration assay schematically shown in Fig. 3-4a. Membranes (10 µm thick with 10 µm pores) were transferred by irreversible bonding to (5:1) PDMS frames (instead of a microfluidic device) with 5 mm circular holes and then released as explained in section II, to obtain free standing membranes (Fig. 3-4b). These were integrated into the migration assay composed of two fluid containing chambers separated by the porous membrane (i.e. in essence a Boyden chamber design). Before cell seeding the membranes were sterilized with isopropanol alcohol.

Cells were seeded in one compartment, whereas in the other compartment medium with a high concentration of a chemical substance known to promote migration of the cells (i.e. a chemo-attractant, Fetal Bovine Serum, FBS) was added [20]. A transient gradient of the chemo-attractant between both compartments establishes by diffusion in the gel, and cell migration (MDA-MB-231 invasive breast cancer cells) through the membrane pores can be assessed by optical inspection of the lower chamber.

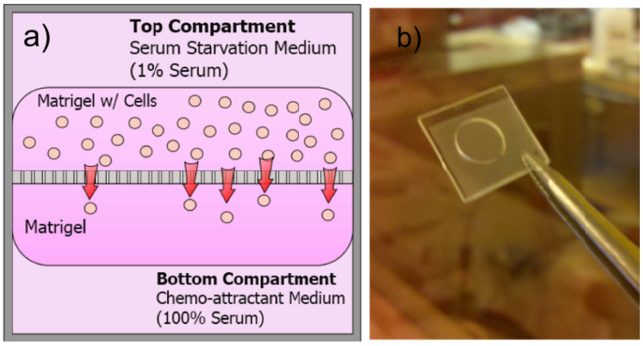

Fig. 3-4 (a) Schematic cross-section of the Chemo-Attractant mediated migration experiments. Two chambers were divided by the porous membrane. Matrigel was applied on the bottom of the porous membrane and a cancer cell-suspended matrigel was applied on top of the membrane. The top compartment was filled with Serum Starvation Medium (Dulbecco's Modified Eagle Medium (Gibco, Grand Island, NY) supplemented with 1% Fetal Bovine Serum, 1% Glutamax and 1% Penicillin/Streptomycin. The bottom compartment was filled with 100% Fetal Bovine Serum as chemo-attractant medium. The setup was placed in an incubator (37 °C, 5% CO2) and incubated for 48 hours. (b) Picture of membranes integrated on 5:1 PDMS frames by irreversible bonding and automatic release in warm water bath.

IV. Results and Discussion

A. Scanning Electron Microscopy

SEM imaging was used to characterize various molded membranes, since optical transparency of PDMS prevents bright-field microscopy to accurately evaluate details of the films (Fig. 4-1a). Samples were observed in an *environmental scanning electron microscope* (ESEM) (1.0-1.2 keV, Quanta 650 FEG, FEI from Hilsboro, USA) which allows observation of polymer surfaces without the need of applying conductive coatings.

SEM images of the successfully fabricated membranes with 10 and 7 µm diameter through-pores are shown in Fig. 4-1b-f. The porous membranes show a difference in surface quality depending on the side of the membrane that is being observed by comparing Fig. 4-1b and c. The membrane side that was molded in contact with the resist coated features shows a smooth curving pore profile and the pore size appears uniform (Fig. 4-1b and f). In contrast, the membrane side facing the dextran layer is observed to be flat and the pores appear to have a variation in sizes (Fig. 4-1c, d and e). To assess the pore quality, several of these membranes were bonded and transferred to PDMS microfluidic channels 100 µm in height and 200-500 µm in width (Fig. 4-1d-f) without showing break or tear. By observing the free-standing membranes on the channels, through porosity can be assessed (Fig. 4-1d). Alternatively, features of the channels in direct contact with the membrane can be viewed directly through the open pores of the membranes (Fig. 4-1e and f). Membranes with smaller pores (~7 µm) and an un-even distribution (center-to-center space is 20 and 40 µm) were also successfully fabricated with ~10 µm tall features (Fig. 4-1f).

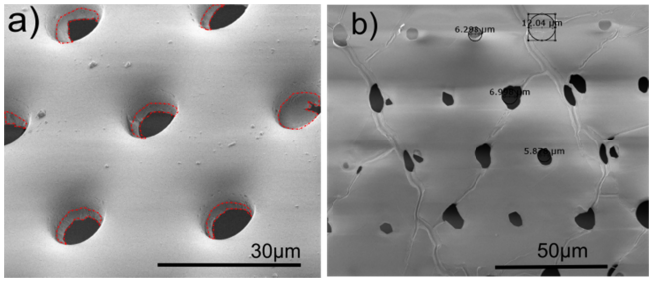

Fig.4-2 (a-b) SEM images of recurrent defects present in the molded membranes. (a) Image (details highlighted in dashed-line) of defects present in the membrane viewed from the mold-facing side. To the right, an ultra-thin PDMS film is observed to cover a molded pore, effectively clogging it. The rest of pores show non-uniformities, these are PDMS excess rims that affect the effective pore size and can promote partial pore clogging. The formation of these thin film and rims is due to incomplete displacement of uncured PDMS during pressing. (b) The membrane, observed from the molded side facing the dextran layer, shows a planar profile and variations in pore size and shape. These variations are due to the defects discussed in Fig. 4-2a. Additionally, cracking marks are observed on the membrane surface. These appear to be superficial and did not compromise mechanical integrity of the film.

Nevertheless, the molded membranes showed a recurrent defect from the fabrication method. The existence of an ultra-thin (~100 nm) PDMS film over several pores on various areas of the molded membrane was observed (Fig. 4-2). This film causes the pores to become partially or completely clogged, thus rendering the pore effectively non-porous (Fig. 4-2a). Additionally, a PDMS excess rim around the open pores was observed (Fig. 4-2a). This excess rim effectively decreases the pore open area and appears, when observing the membrane from the dextran molded side, as variations in the size and shape of the pores (Fig. 4-2b).

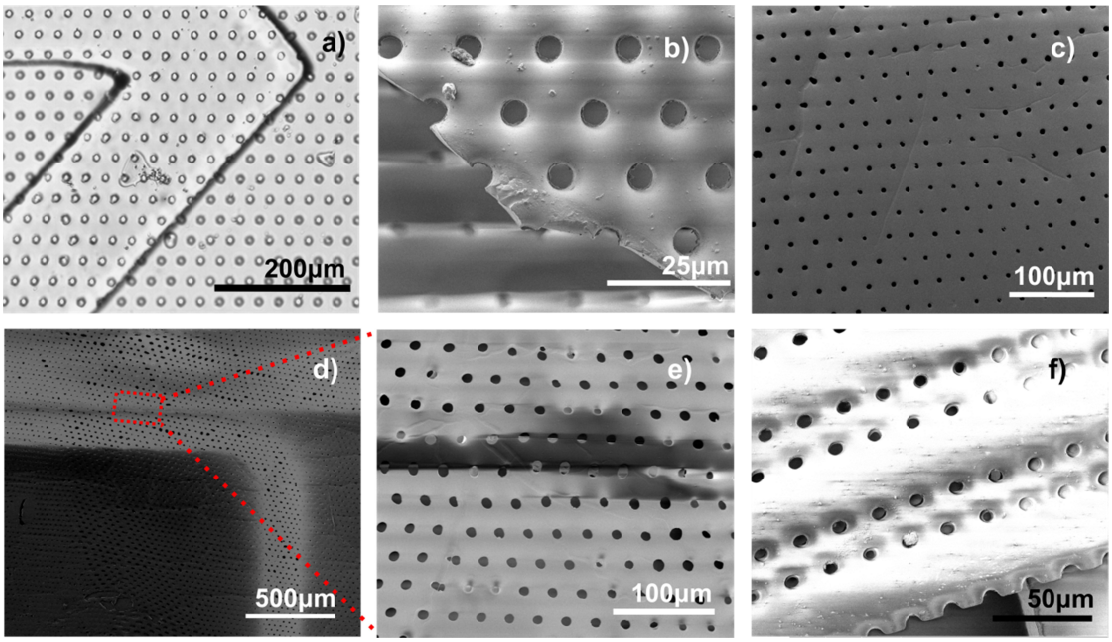

Fig. 4-1 (a) Bright-field micrograph of the porous membrane (10 µm thick & 10 µm pores) bonded to a microfluidic device with a 200 µm wide channel. (b-e) SEM images of succesfully molded ~10 µm thick PDMS membranes with ~10 µm pores. (b) Membrane seen from side facing the pillar mold. The curved profile of the pores and the existence of a thin PDMS rim can be observed. (c,-e) Free standing membrane seen from side facing the dextran, for a sample with a good topographical uniformity can be seen. (d) Membrane bonded to microfluidic channels with widhs of 500 µm and 200 µm; (c-e) membrane standing on 30 µm channel wall; (f) Molded membrane with ~7 µm pores from a similar mold with smaller (7 µm) pillar diameter.

Pore Size & Porosity: The SEM images of seven membrane samples were analyzed using ImageJ (National Institutes of Health, Bethesda, MD) to determine pore size and porosity in case a 10 µm diameter pillar mold was used; these samples correspond to the membranes attached to the microfluidic devices used for posterior fluid characterization. The samples were imaged from the side of the membrane facing the dextran layer. The quantified pore size from the seven samples, as shown in Fig. 4-3a, shows that the observed pore size is smaller (~3-7 µm diameter) than the pillar feature size (10 µm) and varies from sample to sample. Pore sizes that are smaller than the mold pillars as well as pore size variations can be attributed to the defects seen in Fig. 4-2a and b. This bias in an apparent smaller size is obtained from imaging the membranes from only one side. To know the molded pore profile from both sides, the pore size of a membrane imaged from the side facing the mold (Fig. 4-1b) was quantified using the internal and external rim of the pores as reference, the result is

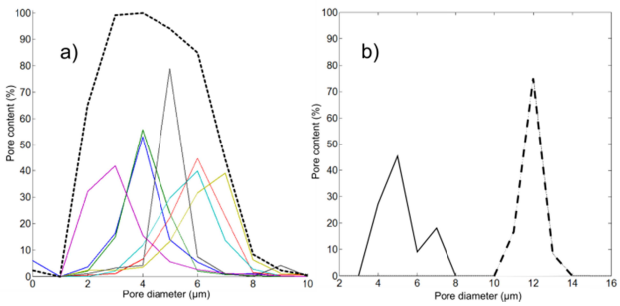

Fig.4-3 (a) Calculated pore diameter of seven different membrane samples, each represented by a different color (10 µm pentagonal pillars molded) from SEM images; samples were observed from the dextran-facing layer. Pore diameter distribution is smaller than pillar feature. Normalized pore content of all the samples is shown in dotted line. (b) Pore diameter of a single sample showing pore-size variations by the analysis of sample with defects as seen in Fig. 4-1b. The molded pore diameter size matches the pillar diameter. The smaller diameters are related to the existence of a PDMS excess rim in the pores.

shown in Fig. 4-3b. The pore profile around 12 µm (dotted line) relates to the expected pore size of 12 µm from the molded pillar profile (i.e. the side of the membrane facing the mold), while the smaller pore size, ~5 µm, is the effective pore size due to the excess rim (i.e. the side of the membrane facing the dextran layer).

The membrane porosity (pore size area vs. total membrane area) was designed to be ~8 %. The SEM characterization shows however that, though all pores are correctly molded from the SU-8 features, the ultra-thin PDMS film which covers different areas of pores, partially or totally clogs them (Fig. 4-2a). In order to give a measure of porosity as a percentage of open pores vs. clogged pores, the SEM images of the small areas (500 x 500 μm^2) of the free-standing membranes from the criss-cross microfluidic devices were analyzed by discerning between open or closed pores. The seven different samples were analyzed and showed porosity variations ranging from 10-92 % open vs. total pores. Partially or fully clogged pore distributions were observed to be localized on various areas of the membrane and no particular difference in distribution or porosity average was observed between samples.

B. Fluid characterization

No devices were observed to delaminate during the fluid experiments confirming good bonding between each PDMS layer of the device. The absolute pressure within the inlet channel of the device during operation (Q_1=Q_2=10 $\mu l \cdot min^{-1}$) was calculated from the equivalent circuit model to be ~0.12 mbar. No leakage from one channel to the other (bypassing the membrane) was observed, providing evidence of good conformal sealing of the membrane to the fluidic channels.

The flow collected of the seven imaged membranes to characterize the porosity at three flow conditions each is plotted in Fig. 4-4 (dotted-colored lines). The ideal flow

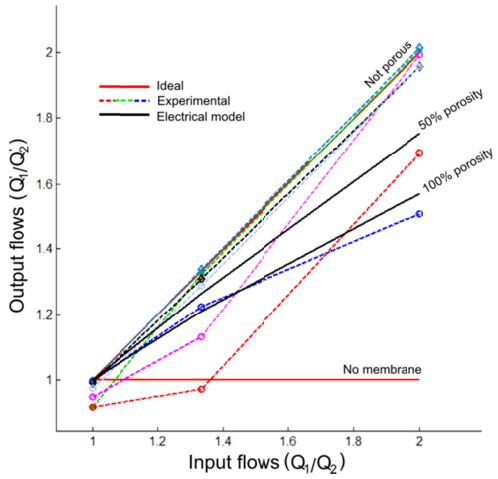

Fig.4-4 Flows collected for each of the seven SEM imaged samples, each represented with a different color of the dashed lines connecting the data dots. The ratio between output flows (Q'_1/Q'_2) vs. input flows (Q_1/Q_2) is used to relate fluidic results to the porosity of the membranes in the samples. The limiting ideal cases (i.e. no membrane and non-porous membrane) have been graphed as the thick red lines. The model results for various porosities (100% and 50%) are shown for comparison as the thick black lines. From the experimental values, two sample groups were obtained, either highly porous or lowly porous. A deviation from the Q_1/Q_2 origin suggests possible sources of error from the setup; due to unmatched resistance of the elements, or errors to retrieve all the flow for its quantization.

conditions for the device for 'Not porous membrane' and 'No membrane' (thick red lines) give the extreme cases and two simulations (50% and 100% open vs. total pores) of the electrical equivalent circuit are plotted to serve for comparison (thick black lines). The experimental data points for each of the flow conditions are connected by a simple linear interpolation. All lines should have the same origin at Q_1/Q_2=1 and, by assuming the membrane resistance (R_{mem}) is invariant during the experiments, they should follow a straight line with a single different slope each. The slope of each line gives a measure of the sample porosity and in turn, this can be compared to the known defined porosity of the circuit model. The plotted results of the samples (Fig. 4-4) show only two extreme cases for the membrane porosity, either almost fully porous (blue and red dotted lines) or almost not-porous (five additional dotted lines). These results show only qualitatively partial agreement with the

SEM observations, since the 'almost fully porous' samples characterized by this method were the same samples with greatest calculated porosity from the SEM characterization (92% open vs. total pores each). The rest of the results that indicate a non-porous membrane are deviant from their previous SEM porosity characterization (contrasting to evaluated porosities of e.g. 88%, 84% and 39%). Additionally, though an apparent absent porosity could be concluded for most of these samples from Fig. 4-2, the collected flows of the DI water channel showed different contents of dye, suggesting some flow through pores in the membranes did occur.

Aside from the porosity evaluation, variations in the experimental setup can be assessed from the results in Fig. 4-4. First, the experimental values can be observed to deviate slightly in origin, indicating possible variations in the experimental setup from sample to sample. These are associated to mismatches of the tubing length and plugging of the blunt needles into the ports of the devices, imprecise manual recollection; drops of fluid remaining at the end of the recollection tubing, and unequal initial experimental conditions; due to a mismatch of the fluid at the end of the tubing. Second, the slope of several samples deviates from an ideal behavior, suggesting a change in membrane porosity during the experiments due to a possible rupture of the clogging thin films covering the pores. Though, this can also be associated to the imprecise nature of the manual recollection; in particular for the small volumes recollected for the duration of each experiment (τ = 50 min), the steady slope of the other 'non-porous' samples suggests the membrane porosity did not change.

C. Porous membranes for cell migration assay

After 48 hours, cells were observed to have migrated only in the samples with presence of the chemo-attractant gradient (Fig. 4-5a and b), thus confirming active migration of cells promoted by the chemo-attractant. Due to the lack of statistical significance from these experiments, adequate degree of porosity of the used membranes cannot be concluded. Nevertheless, by proving invasiveness of cancer cells through the membrane, the fabricated pore size can be assessed when compared to commercial membranes in which pore sizes between 3 -8 µm in diameter are suggested for cancer cell migration assays [21]. This suggested pore size falls within the observed range of the fabricated membranes (3 - 12 µm). Nevertheless, due to the constantly observed smaller pore sizes of the membranes, it could occur that cells were not able to migrate through every pore but only through those that were large enough for them to squeeze through. The cancer cells that migrated can be observed to have a round morphology; consistent with amoeboid-type of cell motility in 3D environments such as matrigel [22]. This type of migration was similarly reported for invasive motion of MDA-MB-231 breast cancer cells through matrigel coated micro-gaps (15 µm) by stimulation with an FBS gradient [20].

D. Discussion on manufacturing process

In this work, we have used a straightforward sequential sacrificial layer release process to address a major technical

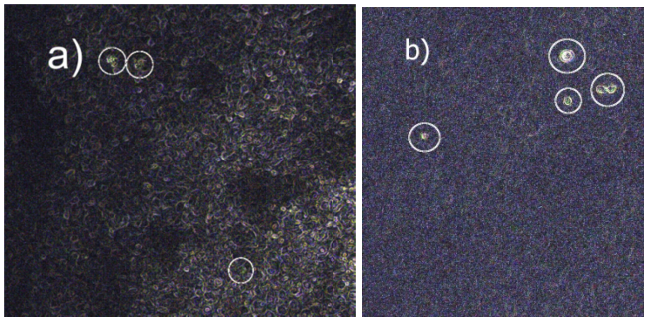

Fig.4-5 (a-b) After 48 hours cells observed to have actively migrated through the porous membrane. Migratory cells were observed by focusing the plane on a bright-field inverted microscope. To recognize better the migratory cells from the background, these have been highlighted and the images manipulated with ImageJ by adjusting the threshold and using the 'find edges' function. The cells appear to have a round morphology, consistent with migration of cancer cells in matrigel. A difference in near and far migration plane from membrane substrate is distinguished between (a) and (b). In (a) the cells that crossed the porous membrane and the cells on the other side of it can be observed simultaneously, whereas in (b) only the migrated cells can be clearly distinguished. Control with serum starvation medium on both sides did not show cell migration.

hurdle of molding large-area, thin micro-porous PDMS membranes, namely the handling and transfer of the membranes. The difficulty of de-molding and transfer of thin elastomeric membranes by traditional and previously reported soft-lithographic techniques is that these heavily rely on manual handling. The problem of handling thin (<50 µm) PDMS membranes are that these tend to flap, stick to themselves and lack the toughness to be handled without break or tear [12]. Additionally, these films tend to stick to flat surfaces, and while peeling them from a structured mold they tend to stretch and interlock with the features thus promoting breaking of the membrane as well as damaging the molding features. With our method, these issues are avoided. De-molding is facilitated by mechanical de-interlocking of the pillar features by dissolving the sacrificial photoresist coating layer of the mold in acetone and also by lubrication of the interface. Furthermore, by applying the thin PDMS film directly onto the dextran coated thick PDMS slab, the film adheres to the slab and therefore can be handled and transported without breaking or sticking, and at the same time it can be released in a controlled manner by dissolving the dextran sacrificial layer in water [17]. It is essential that the two release steps can be carried out independently, through the choice of the particular sacrificial layer materials. Though PDMS swelling by acetone exposure is known to be ~1% this is reversible and no negative effects as a result of the swelling were observed.

The use of the positive resist as sacrificial layer has advantages compared to commonly used anti-stiction coatings in soft-lithography, such as silane based self-assembled-monolayers (SAM's). Aside from the reported difficulty to successfully deposit anti-stiction coatings on SU-8 molds [23], when transferring a thin PDMS layer with through features by bonding to a device by activation with oxygen rich plasma, SAM coatings are disrupted by the plasma therefore potentially promoting unwanted adhesion between the final device and the mold. Photoresist similarly

serves as an anti-adhesion coating to PDMS, but has the benefit that it is not affected by oxygen plasma [7].

By having an exposed PDMS membrane over the dextran sacrificial layer it is possible to transfer and bond the membrane to a silicone (PDMS) or glass substrate by applying a surface treatment with oxygen rich plasma. Alternatively a corona treatment can be used. We note that although some of the dextran was directly exposed to either plasma or corona (through the openings of the pores on the membrane) this showed no negative effect on its ability to dissolve. Additionally, we observed that dextran has a good adhesion with PDMS such that cleaning of the membrane can be performed by removal of dust particles with scotch-tape. To achieve successful release of the thin membrane from the PDMS slab, we have observed that the hydrophobic nature of the PDMS surfaces diminishes water's ability to creep into the PDMS-PDMS interface. To aid the wettability of PDMS, using a solution of Tween 20 (0.05%) in water was found helpful as reported in [17]. In addition, it was also observed that the PDMS that was coated with the dextran layer after surface oxidation remains temporally hydrophilic after the dextran layer is dissolved. A similar effect was previously reported after etching of an Al coating on an Ar plasma activated PDMS surface [24], therefore water can successfully creep into the PDMS-dextran-PDMS interface when exposed manually by mechanical delamination of the surrounding area. By immersion of the layer sandwich in warm water for sufficiently long time the dissolution process of dextran is enhanced. The release is performed automatically by buoyancy of the PDMS freeing from the dextran layer in this way avoiding overall manual handling. Special care must be taken with large free standing membranes in which case stirring of the bath during lift-off can result in stresses that can create micro-tears in the membrane.

The process was optimized to create through features by pressing the uncured PDMS film onto the photoresist-coated mold features by using a set of clamps. The force exerted by the clamps has been calculated to be ~5-10 N. Smaller forces were ineffective to create through features on the thin film and instead micro-wells with the form of the features are molded. Similarly, an immediate curing step at high temperature after initial pressing was observed to promote films of higher thickness than that of the molding features. Therefore, an overnight curing step at room temperature (for at least 12 hrs.) was needed to let the PDMS creep out of the gap between the mold and dextran coated PDMS slab, and a subsequent final curing step before releasing the clamping pressure and de-molding was required to achieve complete curing of the PDMS membrane.

For a variety of mold features, ranging from 7 µm diameter pillars to 100 µm wide channels with various heights (10 µm's to 100 µm's), this clamping force did not cause any damage to the mold features. It was observed, however, that the robustness of the mold to handling depended strongly on the correct processing of the SU-8, in particular for small and high aspect ratio features. A clear review on SU-8 processing is given in [25]. Our compression method has been shown to effectively mold and release membranes with 7 µm pentagonal features (with an aspect ratio of about 1) which is the minimum feature size present on the lithography mask that was used. The limiting factor to mold smaller through features is determined by the resolution of the lithography mask used, the SU-8 feature dimensions, namely the aspect ratio of the features, feature pitch and the thickness of the SU-8 coating, and the microposit sacrificial layer coating thickness. Thickness and through feature size of the membranes scales similarly, i.e. a small aspect ratio (~1:1) of the mold features

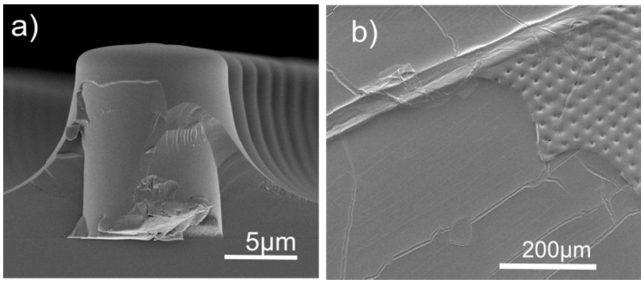

Fig.4-6 (a) SEM image showing the spin coated photoresist sacrificial coating on the SU8 features of the mold. A ~2 nm Pt/Pd layer was sputtered on the mold and visualization was done using a FEI XL40 FEG-SEM for better contrast. The photoresist coating is observed to be non-uniform therefore affecting the molded pore profile. Though this non-uniform coating is un-desirable, it aids the de-molding procedure. The effect of this profile can be observed in Fig. 4-2a. (b) PDMS substrate on which the dextran layer was spin coated after membrane lift-off reveals cracking of the substrate. These cracks can be explained by stresses generated during processing, such as dextran layer bake which promotes both intrinsic and thermal stresses during deposition. The impact of these cracks on the final membrane was diminished by slow heating and cooling of the substrate during dextran deposition.

is preferred to avoid breaking off of the features. This is consistent with previous reports on molding of thin elastomeric membranes [12].

The membrane thickness was found to be uniform and the same as the pillar height. From our SEM characterization it appears that the resist affects the molding resolution of the pores by increasing the molded diameter by twice the photoresist coating thickness (~1 µm) (Fig. 4-6a), thus pore size is observed to be approximately 12 µm instead of 10 µm, moreover the pillar shape appears to be more round instead of pentagonal (Fig. 4-1b and 4-2a). Though the membrane and pore profile is observed to be smooth down to the micro scale on both sides of the final membrane, the pore profile appears affected by local non-uniformities of the resist coating on the bottom and top of the pillar features due to hydrodynamic effects as can be seen in Fig. 4-6a.

The side of the membrane facing the dextran layer was observed to be smooth and flat (Fig. 4-1c and e), this result is in concordance to what was previously shown of dextran to have a low surface roughness (0.27 nm rms) when coated as a uniform layer (~nm's-1 µm's) on flat substrates [17]. Nevertheless topographical defects were observed on the molded membranes (Fig. 4-2b) associated with the cracking of the dextran layer (Fig. 4-6b). These cracks could be induced by intrinsic stresses during processing, such as drying of the dextran deposited layer by thermal processing.

Alternatively drying can be pursued by blowing nitrogen on the spin coated slab or by vacuum. The PDMS slab base-to-curing agent mixture ratio was observed to influence the formation of cracks. Stiffer PDMS (i.e. 10:1) decreased the overall topographical defect formation effect; however, this negatively impacted the reliability of molding through features by promoting the formation of an ultra-thin film clogging the pores. Henceforth, a softer (15:1) PDMS substrate was used and cracking was diminished by long ramp-up and ramp-down of the temperature source to dry the dextran layer on top. The appearance of these defects was therefore overall diminished and the remaining surface details were not observed to cause any tearing or breaking of the membranes when suspended over PDMS channels ~1 mm in width.

V. Conclusions and Future work

In this work, a simple, useful and robust method to fabricate and transfer thin microporous PDMS membranes was demonstrated. The method uses a sequential mold, release, de-mold and de-bond strategy similar to that used for MEMS processing. This method avoids manual handling which is a source of tearing and breaking of the membrane in standard soft-lithographic processes, and it substantially eases de-molding. Though, we have demonstrated the fabrication of thin ≤10 µm micro-porous (7-10 µm diameter, ~20-30 µm pitch) large area (3 cm x 1 cm) membranes, the results were not perfect as the existence of a thin PDMS film over many areas of the membrane partially or fully clogs the pores, thus rendering these areas effectively not porous.

Aside, the method was observed suitable for fabricating a wider range of features (e.g. micro-channels), and is scalable to wafer-size processing to increase throughput. A crucial advantage of this process is that the mold used is made from SU-8 which is a common photoresist for high aspect ratio features, and is readily available and easy to process using standard photolithography. Additionally, this mold was proven to be reusable for more than five times. As a result fabrication of the mold and the membrane fabrication process is standard, cost effective and moreover, relies solely on readily available equipment, in contrast to silicon molds with high aspect ratio features that rely on expensive and specialized equipment such as *Deep Reactive Ion Etchers* (DRIE).

The fabricated membranes were successfully and easily bonded and transferred to PDMS micro-fluidic chips on which different properties were tested. SEM imaging characterization was used to assess membrane surface quality and feature dimensions, showing an asymmetric pore profile and various areas with a remaining ultra-thin (~100 nm) PDMS film covering many of the pores, leading to only partial porosity of the membrane. To address the formation (or etching) of this undesirable film, refinement of the current process and/or additional processing steps could be explored such as:

(i) Using molding features with higher aspect ratio (h/w~ 2-5) and, by spin coating a thin (~10um) PDMS layer directly on the dextran coated slab, stamp and press this thin layer against the coated mold until fully cured; similarly to the protocol given in [5].

(ii) Using slightly higher pillar features (h/w~ 2) and spin coating a mixture of solvent and PDMS directly on the coated mold, then directly pressing with the dextran coated slab until fully cured; similar to [10].

(iii) Post-processing the membrane using a dry-etching step before final lift-off. Since the excess film is much thinner than the membrane, a quick PDMS dry etching process and a time etch-stop technique could be potentially implemented [7].

(iv) Post-processing the membrane using a wet-etching step. Stability of the dextran sacrificial layer to the PDMS etching-chemistry is critical to prevent accidental lift-off. Various wet-etching techniques to etch PDMS residues and in-situ patterning of PDMS microfluidic devices have been presented [26, 27].

Fluid characterization of porosity did not give reliable results with the methodology used due to miss-calibration of the experimental setup, variations in the manual recollection method; which were aggravated by the small volume recollected, small number of experiments performed and due to the observed pore size variations that cannot be differentiated from porosity variations with this method. Though, from the experiments the membranes showed mechanical sturdiness to a difference in pressure; which caused them to deflect, and none were observed to rupture. Nevertheless, the thin films clogging the pores were not observed to break during the experiments, which would have increased the porosity. A theoretical and experimental study would be necessary to predict the conditions to break this thin film while maintaining integrity of the membrane.

Finally, though PDMS is already known to be bio-compatible, we were able to prove the use of these membranes for culturing and chemotactic migration of cells, showing their potential for the development of microfluidic bio-assays and in particular for Organ-on-chip platforms in standard micro-fabrication laboratories.

Acknowledgments

This project was done for fulfillment of the degree of MSc. Biomedical Engineering at the Delft University of Technology. This work used the Miplaza facilities at Philips Research, Eindhoven. The author would like to thank all the other authors for their collaboration and support. The authors additionally would like to thank Angel Savov, Hossein Eslami, Ye Wang, Agnese Ravetto and the Microsystems Group at TU/e for their support.

References

1. De Jong, J., et al. "Membranes and microfluidics: a review." *Lab on a Chip* 6.9 (2006): 1125-1139.
2. Chueh, Bor-han, et al. "Leakage-free bonding of porous membranes into layered microfluidic array systems." *Analytical chemistry* 79.9 (2007): 3504-3508.
3. Berthier, Erwin, et al. "Engineers are from PDMS-land, Biologists are from Polystyrenia." *Lab on a Chip* 12.7 (2012): 1224-1237.
4. Mukhopadhyay, Rajendrani. "When PDMS isn't the best." *Analytical chemistry* 79.9 (2007): 3248-3253.

5. Huh, Dongeun, et al. "Microfabrication of human organs-on-chips." *Nature protocols* 8.11 (2013): 2135-2157.
6. Dongeun Huh, et al. Reconstituting organ-level lung functions on a chip. *Science*, 328(5986):1662–1668, 2010.
7. Chen, Weiqiang, et al. "Photolithographic surface micromachining of polydimethylsiloxane (PDMS)." *Lab on a Chip* 12.2 (2012): 391-395.
8. Chen, Weiqiang, et al. "Surface-Micromachined Microfiltration Membranes for Efficient Isolation and Functional Immunophenotyping of Subpopulations of Immune Cells." *Advanced healthcare materials* 2.7 (2013): 965-975.
9. Koschwanez, John H., et al. "Thin PDMS films using long spin times or tert-butyl alcohol as a solvent." *PLoS one* 4.2 (2009): e4572.
10. Wei, Huibin, et al. "Particle sorting using a porous membrane in a microfluidic device." *Lab on a chip* 11.2 (2011): 238-245
11. Thangawng, Abel L., et al. "An ultra-thin PDMS membrane as a bio/micro–nano interface: fabrication and characterization." *Biomedical microdevices* 9.4 (2007): 587-595.
12. Jackman, Rebecca J., et al. "Using elastomeric membranes as dry resists and for dry lift-off." *Langmuir* 15.8 (1999): 2973-2984.
13. Masters, Thomas, et al. "Easy Fabrication of Thin Membranes with Through Holes. Application to Protein Patterning." *PloS one* 7.8 (2012): e44261.
14. Lau, Kia Hian, et al. "Releasing high aspect ratio SU-8 microstructures using AZ photoresist as a sacrificial layer on metallized Si substrates." *Microsystem technologies* 19.11 (2013): 1863-1871.
15. Luo, Cheng, et al. "Releasing SU-8 structures using polystyrene as a sacrificial material." *Sensors and Actuators A: Physical* 114.1 (2004): 123-128.
16. Addae-Mensah, et al. "Poly (vinyl alcohol) as a structure release layer for the microfabrication of polymer composite structures." *Journal of Micromechanics and Microengineering* 17.7 (2007): N41.
17. Linder, Vincent, et al. "Water-Soluble Sacrificial Layers for Surface Micromachining." *Small* 1.7 (2005): 730-736.
18. VanDersarl, et al. "Rapid spatial and temporal controlled signal delivery over large cell culture areas." *Lab on a Chip* 11.18 (2011): 3057-3063.
19. Chung, Henry H., et al. "Highly permeable silicon membranes for shear free chemotaxis and rapid cell labeling." *Lab on a Chip* (2014).
20. Chaw, K. C., et al. "Matrigel coated polydimethylsiloxane based microfluidic devices for studying metastatic and non-metastatic cancer cell invasion and migration." Biomedical microdevices 9.4 (2007): 597-602.
21. Life Sciences Corning Inc. Transwell permeable supports selection and use guide. 2010.
22. Paňková, K., et al. "The molecular mechanisms of transition between mesenchymal and amoeboid invasiveness in tumor cells." *Cellular and molecular life sciences* 67.1 (2010): 63-71.
23. Moresco, Jacob, et al. "Improved anti-stiction coating of SU-8 molds." Sensors and Actuators B: Chemical 145.2 (2010): 698-701.
24. Zhou, Jinwen, et al. "Recent developments in PDMS surface modification for microfluidic devices." *Electrophoresis* 31.1 (2010): 2-16.
25. Del Campo, A., and C. Greiner. "SU-8: a photoresist for high-aspect-ratio and 3D submicron lithography." *Journal of Micromechanics and Microengineering* 17.6 (2007): R81.
26. Balakrisnan, Bavani, et al. "Patterning PDMS using a combination of wet and dry etching." *Journal of Micromechanics and Microengineering* 19.4 (2009): 047002.
27. Takayama, Shuichi, et al. "Topographical micropatterning of poly (dimethylsiloxane) using laminar flows of liquids in capillaries." *Advanced materials* 13.8 (2001): 570-574.

Chapter 6

Recommendations

On the basis of the results and discussion presented, several recommendations are drawn for possible improvements of the membrane fabrication process, its characterization and for future developed membranes for a Cancer-on-Chip device.

Membrane Fabrication

- The formation of the ultra-thin PDMS layers clogging the pores should be assessed systematically and on the basis of understanding the PDMS displacement phenomena from the molding features. The fact that through pores sections are obtained with this process shows that it is possible its refinement to render a uniform layer with the desired porosity. The aspect ratio and size of the molding features, applied pressure and uniformity of the dextran layer would be the main variables to optimize.
- To render the membranes fully porous, a final PDMS dry etching step could be implemented as a post-processing step of the current fabrication method. Practical considerations; such as chemical compatibility of dry etching chemistries of PDMS, must be reviewed to assess whether such a step is feasible as a quick final step with a simple time etch-stop strategy.
- Various forms of PDMS wet etching post-processing steps could be implemented to render the membrane fully porous such as: (i) Directly exposing the membrane adhered the PDMS carrier slab by the dextran layer to a wet etching bath. The chemical stability of the dextran sacrificial layer would need to be assessed to avoid accidental lift-off. (ii) To avoid over exposure of the membrane and due to the asymmetric pore profiles, the membranes could be wet-etched while free-standing on frames. A uniformly deposited etch-stop mask (such as a Aluminum) could be used to protect the correctly molded side while leaving the side of the membrane containing the ultra-thin films clogging the pores directly exposed to an appropriate wet-etching solution. (iii) The side of the membrane presenting the pore-clogging ultra-thin films could be exposed to a laminar flow of appropriate PDMS-etchant in-situ (i.e. already bonded on the final microfluidic device).

- The thin film clogging the pores in the membrane could be burst open by applying a pressure differential between both sides of the membrane. To calculate at which pressure differential and which experimental setup would be needed, mechanical considerations for fracture of thin elastic materials need to be drawn. In the basis of these calculations, a set of well planned bulging tests could confirm if it is possible to post-process the membrane and open the clogged pores with this technique, or if the membrane itself would rupture before any significant change in porosity is achieved.
- The influence of processing parameters on cracking could be well understood and avoided with an extended study on the mechanics of stresses in thin films. A carefully designed set of experiments could prove if the observed cracks on the membrane are either possible sources of failure or if they are uniquely the negative mold of the cracks from the underlying brittle substrate.
- Though the methodology for fabrication of a membrane here presented has limited processing variables, the use of sacrificial layers to alleviate problems and enhance throughput of soft-lithographic techniques could be coupled to other variants of fabrication processes for porous membranes. For example, the de-molding problem of a spin-coated diluted PDMS mixture directly on high aspect ratio features could be potentially tackled by incorporating a lift-off procedure.

Characterization

- SEM imaging with an ESEM proved an excellent way to determine the surface quality of the fabricated membranes, nevertheless, the use of an appropriate conductive coating for SEM imaging is recommended to ensure correct inspection of the membrane characteristics when possible.
- Though the fluid characterization methodology used in this work did not provide a reliable assessment of successful fabrication of the membranes (i.e. porosity). This can be attributed to imperfections and non accounted details in the experimental setup such as; the manual nature of fluid recollection method, too small volumes recollected and few experiments conducted. Nevertheless, membranes with a consistent porosity quality do could be assessed before their experimental use with a variant of this simple and fast methodology.
- A simple, yet well defined electrical resistance model can provide a simple and handy way to asses the fluid implications of a membrane as a permeable barrier. Such a model is worthy of developing and useful particularly if the membranes are standard in size. The point of the study would be to understand the fluid implications of diffusive or advective flow through the membrane for stimulation of cells.
- Though the cell and fluid characterization have independently shown these membranes could function as a suitable substrate for a microfluidic migration assay, the porosity reliability problem from the developed fabrication method must be addressed before any further cell work is done.

Appendix A

Detailed Fabrication Process Flow

Mold fabrication (Timing: ≈2.5 hr)

A specially designed SU-8 mold with regularly distributed pillars was made with standard photo-lithographic techniques.

Mask design:
A dark field chrome on glass mask (Techno-Mask, Eindhoven, The Netherlands) with pentagonal features in a hexagonal lattice fashion (pillar outer diameter 10, center-to-center pitch 30μm) is used for fabrication of the SU-8 mold features. The pattern consists of an array of pillars spanning a rectangular area of 1.0 cm vs 3.0 cm.
Note: The pattern array used spawns only a limited region of the mask, therefore the wafers were cut in four with a diamond-tip pen, cleaned and then processed. Alternatively the full wafer can be processed and then cut; though caution must be taken not to break the features of interest.

Substrate preparation:
A wafer is cleaned by subsequent rinsing with acetone, ethanol and iso-propanol alcohol (IPA). Before IPA dries in air, manual drying is performed with a nitrogen gun. Final clean and increasing of adhesion is promoted with a UV-ozone exposure step (≈15 min).

Spin-coat and pattern SU-8 2010

- Dispense SU-8 2010 on the wafer piece and spin coat a 10 μm thin layer by first setting a spinning speed for 500 rpm (110 rpm/s) for 15 sec and ramping up to 1700 rpm (330 rpm/s) for 35 sec.
- Bring the coated substrate to a hot plate and soft bake for 3 min at 95 degC. After this, leave the mold to cool-down to room temperature for 5 min.

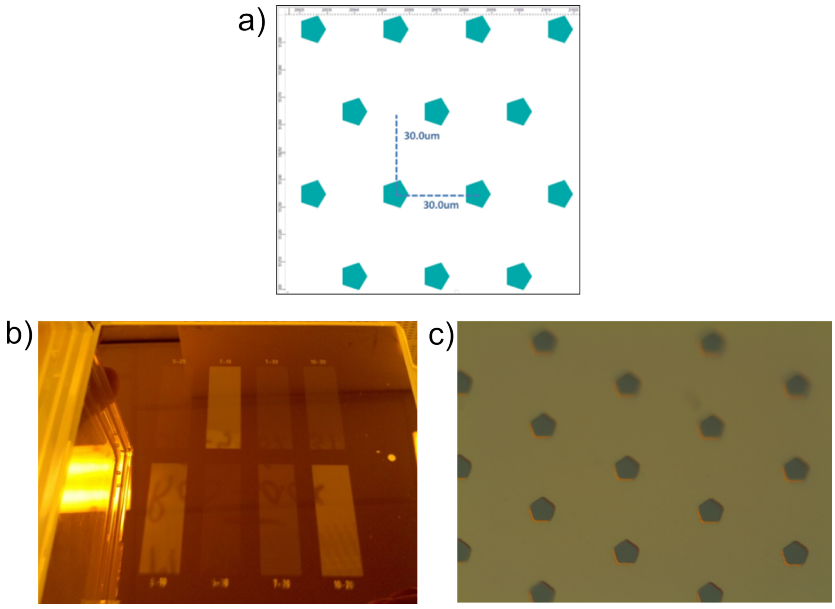

Figure A-1: *(a) The pillar array was created in a graphic aided software and it consists of an array of 1 cm x 3 cm of 10 μm pentagonal pillars with hexagonal lattice fashion interspacing of 30 μm. (b) A chrome-on-glass mask is used for its sub-micron resolution necessary to correctly resolve the pentagonal pillar profile. Commonly used acetate masks for microfluidics are not suitable as these have minimum feature resolutions of ≈20 μm. (c) Micrograph showing as detail the pillar array.*

- Bring the clean mask in contact with the coated layer and expose to UV for 45 sec (intensity of the lamp ≈11.4 mW/cm^2).
  Note: The mask must be centered on the coated substrate so that the features are not exposed on the non-uniform edge of the substrate; this effect is common for spincoated layers.
- Immediately after exposure, bring the coated and exposed substrate to a hot plate for a Post Exposure Bake for 4 min at 95 degC. Leave the substrate to cool-down to room temperature for 5 min before further processing.
- Carefully place the mold on negative resist developer (Mr. Dev 6000) and leave for approximately 10 min; more time might be needed.
  Note: Agitation might result in breaking of the pillars. Mild stirring with a magnetic rod is preferred to avoid break of pillars.
- After complete development, clean the mold with Ipa & gentle dry with nitrogen gun.
- A hard bake step is done for 30 min at 200 degC to improve the mechanical properties of the mold and its geometrical features.

Resist spin-coat S1813 JX

- Place the SU-8 on silicon mold on the vacuum chuck of the spin-coater and dispense ≈ 700 μl of the positive photoresist with a pipette to cover most, ≈ 90 %, of the substrate.
  Note: Avoid dispensing directly on the features as this traps bubbles.

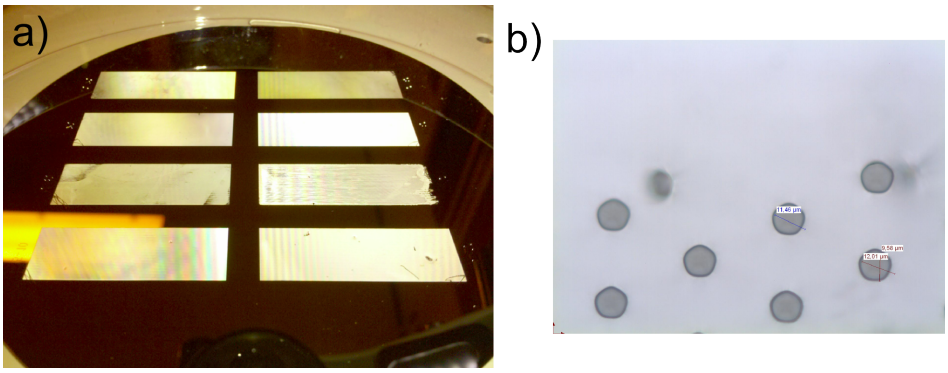

Figure A-2: *The SU-8 on silicon mold as fabricated from exposure through the chrome-on-glass mask. (a) Here, different sizes and geometries of features were fabricated on a single wafer. Evenly spaced arrays of 7 and 10um pillars; inter-pillar spacing from 20 to 30um, showed the best reproducibility. The mold can be cut with a diamond-tip pen and cleaned; as explained by subsequent rinsing, before usage for molding. (b) Micrograph (50x) of the pillar pattern in SU-8. Note that the SU-8 features have lower definition than the mask features used for exposure in Figure A-1. For this picture it can be seen the pentagonal features are more rounded. This can be attributed to the long-exposure dose which significantly changes the cross-link area.*

- Spin coat the resist first for 10 sec at 500 rpm (110 rpm/s) and then ramp up for 30 sec at 4000 rpm (330 rpm/s).
- By avoiding contact with the coated layer and the features as much as possible, place the coated mold on a hot plate for 5 min at 110 C. Take the mold off the plate and leave to cool down to room temperature for ≈ 5 min.
- Expose the coated mold with the exposure tool for ≈ 25 sec and store in a clean petri dish until further use.

PDMS slab carrier fabrication (Timing: ≈12hr)

- Mix, degass and pour a (15:1) PDMS mixture onto a clean wafer to fabricate a uniform (≈ 4mm) thick layer. Leave the prepolymer to cure at room temperature on a leveled surface overnight or alternatively on a leveled hot plate at 70 degrees for ≈ 3hr.
  Note: The wafer can be previously silanized or coated with a surfactant layer of detergent and water mixture to avoid the cured PDMS from sticking to the wafer.
  Notes: Before any manual or peel off, the set is left to cool down to room temperature.
- Cut the peeled PDMS layer as a rectangular slab (2.5 cm X 4.0 cm) and also the corners on 45 deg angles.
- Reversibly attach the aligned slab to a clean glass microscope slide.
  Critical: Non-conformal seal of the PDMS slab on the slide can promote complete failure of the slab substrate after deposition of the dextran layer due to developed stresses. This is observed as de-lamination of the PDMS slab from the microscope slide due to excessive bending of the substrate.

Dextran coating on PDMS carrier (Timing: ≈2hr)

Dextran preparation:
The dextran water mixture was prepared as reported in [25]. A 20% (w/v) solution is made by mixing 20 gr dextran 70 (MW: 70 kDa) in 100 ml DI water in a vial and stirring with magnetic rod while on a hot plate at 90 degC for approximately 1 hr. The mixture must be left to cool down to room temperature before use.

- First, the PDMS slab attached to the microscope slide is treated by a 20W air plasma for 35 sec.

- Then, once the slab is placed on the vacuum chuck of the spin coater, pipette ≈ 700 μl on the surface of the PDMS to cover most of its surface (Figure A-3a).

- Spin coat the deposited layer first 15 sec at 500rpm (110 rpm/s) and ramp up to 4000rpm (330rpm/s) for 30 sec (Figure A-3b).
  Note: The spin coated layer should appear uniform, transparent and fully covering the PDMS surface. If the layer is missing to cover areas of the PDMS, the surface can be rinsed with DI water and deposition of the dextran solution can be again attempted.

- By handling the slab from the microscope slide, bring the coated slab to a hot plate at 80 C and leave for 1 hr. A ramp down of ≈1 hr is needed to bring the slab to room temperature before further processing. After this, the slab can be placed inside a clean petri dish until further use.
  Critical: Two glass petri dishes lined with absorbent non-fibrous tissue are placed on the hot plate. The slab is placed inside this set to avoid contact with room temperature conditions and promote controlled evaporation of the water content of the deposited layer. The tissue must never touch the coated layer. Before bringing the slab outside of the dishes, a ramp down step until reaching room temperature is done for ≈1 hr. A sufficiently long ramp down and correct evaporation process of the water in the coating layer promotes a defect-free translucent layer on the PDMS slab.

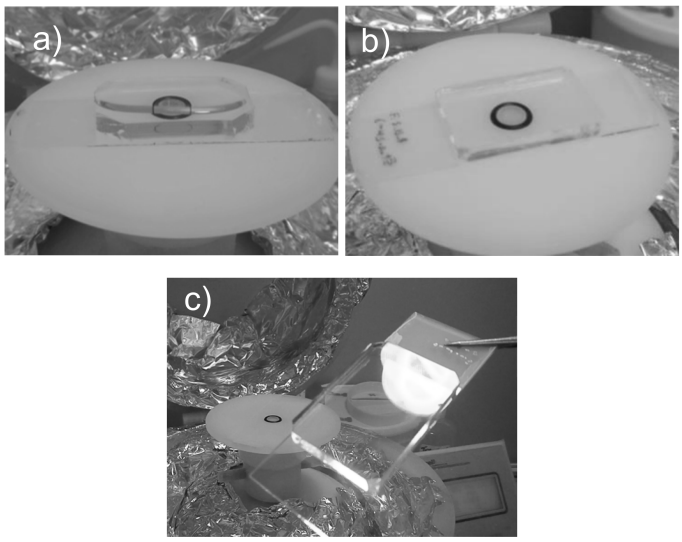

Figure A-3: *(a)The dextran mixture is deposited with a pipette to cover most area of the surface while avoiding formation of bubbles. The surface, made temporally hydrophilic by air plasma treatment, shows good wetting properties. (b) After spin-coating, the dextran layer has spread evenly, creating a thin, uniform layer of water-dextran mixture. (c) The PDMS slab is removed from the chuck and handled uniquely by the microscope slide onto which the slab is reversibly bonded. Defects of the dextran coating layer, such as incomplete covering, can be assessed by simple inspection. Evaporation of the water solvent on the layer completes the deposition process.*

Molding procedure (Timing: ≈13hr)

- Prepare a mixture of 10:1 PDMS, degas until no bubbles are present in the mixture and carefully dispense ≈ 2 gr on the photoresist coated mold.
  Note: PDMS should not be poured directly on the features, this leads to trapping air bubbles in the mixture. Instead, PDMS is dispensed next to the features and left to flow to cover the features (Figure A-4).

Figure A-4: *(left) An uncured, degassed, 10:1 PDMS mixture is poured on an area of the mold cont aining no features. (middle & right) PDMS is left to flow to achieve complete coverage of the full array with features. This prevents formation of air traps.*
Note: *Avoid pouring directly on features, and wait for PDMS to wet the feature surface.*

- Bring the thick PDMS dextran coated slab to the PDMS covered features (dextran layer facing the uncured PDMS) and lay down gently on the PDMS. After full contact, push gently on the slab to displace the uncured PDMS (Figure A-5).

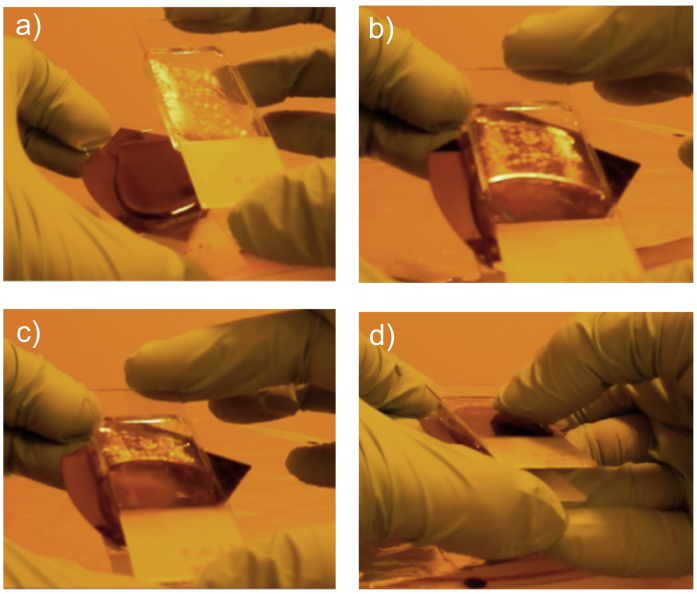

Figure A-5: *(a-d) The PDMS slab; reversibly bonded to a microscope slide, is brought to contact with the uncured PDMS layer on the prepared SU8 mold by carefully laying the slab. A final gentle push helps displace excessive uncured PDMS at the interface.*
Note: *Placing should be done by tilting; this avoids trapping air between uncured PDMS and dextran.*

- Apply constant pressure between mold and slab (microscope slide) and secure it in position to avoid sliding of surfaces. Then, leave the set pressed for overnight curing (≈12 hr) at room temperature (Figure A-6).

- After overnight curing, bring the pressed sandwich in a convective oven for >1 hr at 70 degC.
Critical: The pressure between mold and slab should not be released before complete curing of the molded PDMS layer.

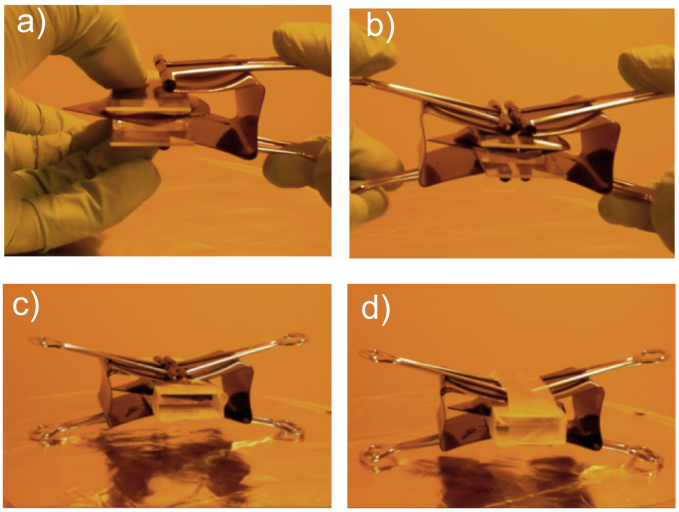

Figure A-6: *(a-b) The previously prepared slab with dextran coating sitting on uncured PDMS is gently set between two clamps, one clamp at a time. Handling of the clamps must be so that full clamping force is only applied once the mold and slab are in their final positions. An additional 4 mm thick 15:1 PDMS slab reversibly bonded to a microscope slide were attached to the flat back side of the mold to increase molding pressure of the clamp set.*
Note: *The middle of the molding array should be symmetric and centered to the clamps contact points. The slab and mold might slide away from each other, due to lubrication from the uncured PDMS, for this reason the force excerted by both clamps must be applied simultaneously and must be centered. (c-d) After the clamps have been positioned and released on the mold and slab, these must be secured in position.*
Note: *Scotch tape was observed to be enough to prevent any undesired sliding of the molding sandwich.*

De-molding & Transfer of membrane (Timing: ≈2hr)

- The de-molding process begins by carefully releasing the clamp set and freeing the stamped mold from tape and excess PDMS holding it in place.
  Critical: During the whole de-molding process any stress between the PDMS slab and the Si substrate should be avoided as these can produce undesired peel and tear of the membrane.

- Remove the microscope slide on top of the PDMS slab by carefully inserting a scalpel blade or fine tweezers and using these as a lever. The corners are first un-attached and further peel can proceed by letting the blade in the interface.
  Note: Dispensing a drop of ethanol reduces adhesion and promotes automatic de-bonding.

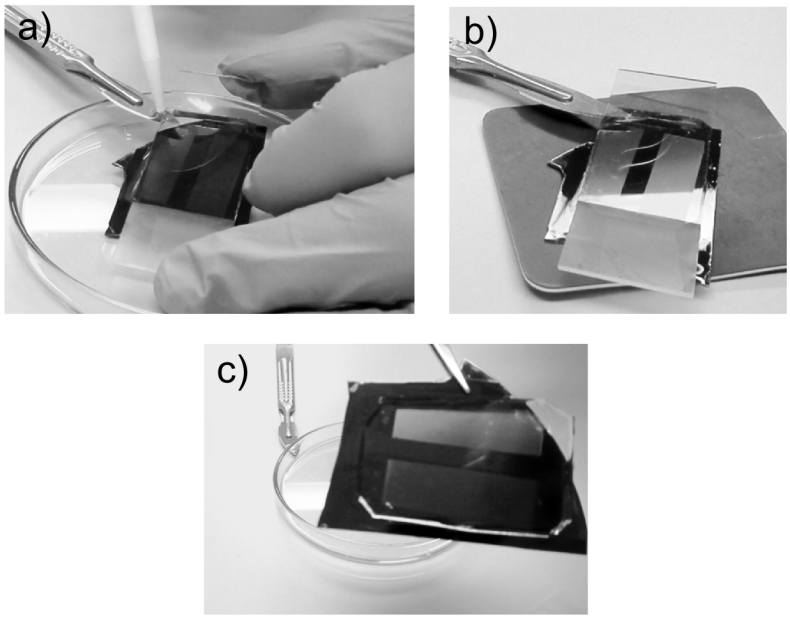

Figure A-7: *(a) Detachment of the microscope slide from the PDMS slab begins by inserting the blade of a scalpel in the corners of the interface, and gently using it as a lever to promote partial de-bonding of the perimeter. (b) By positioning the scalpel blade on a stable surface, it can be left to on its own slowly as a lever thus avoiding use of excess force for de-bonding. A drop of ethanol can be deposited on the scalpel blade or the interface to further aid de-bonding.* ***Note:*** *Ethanol must be dispensed carefully to avoid wetting of the interface in contact with the mold; this is to avoid accidental etching of the dextran layer with ethanol.*
(c) After successful release ethanol should be dried by blow drying or use of a non-fibrous tissue. The Slab must be well adhered to the mold.
Note: *Lamination and detatchement of the slab from the mold could be a sign of unsuccesfull curing of the membrane interface holding them in position.*

- With a sharp and clean blade, make an incision and cut directly on the mold all around the perimeter layer of the slab. A layer of PDMS is normally found around the slab as it is excess which was squeezed out of the mold. Cutting into the mold through this excess PDMS creates openings for acetone to wet the interface between slab and mold.

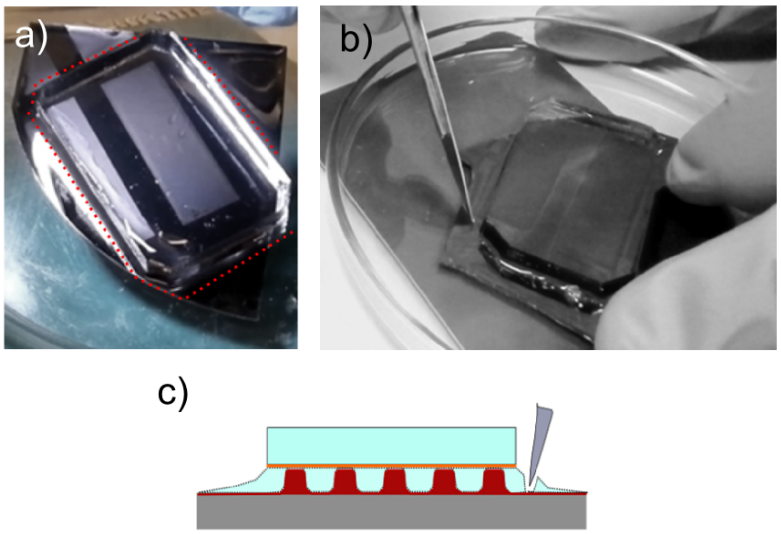

Figure A-8: *(a-b) With the clean blade, the perimeter of the mold surrounding the PDMS slab is cut, therefore making access holes to acetone etchant through any excess PDMS which might have creped between the slab and mold. Damage of the underlying photo-resist coating is not a concern. (c) Schematic drawing showing the position in which the access holes are created. Making these cuts too near to the molding features might promote accidental de-molding of the membrane by mechanical stress. The slab therefore must be preferentially bigger and well centered from the molding array.*
Note: *The mold is tightly held by pressing on the hard substrate; handling by the PDMS carrier can promote accidental de-molding.*

- Place the mold and slab on a glass beaker and dispense acetone at their interface. To promote de-molding, a pair of fine tweezers is used as a lever at the corner and sections of the mold without features.
  Critical: While de-molding requires physical peel-off of the PDMS carrier, this is done to promote acetone wetting of the interface which is sufficient to free the membrane and slab from the mold, thus no excess force is required to peel-off the slab.

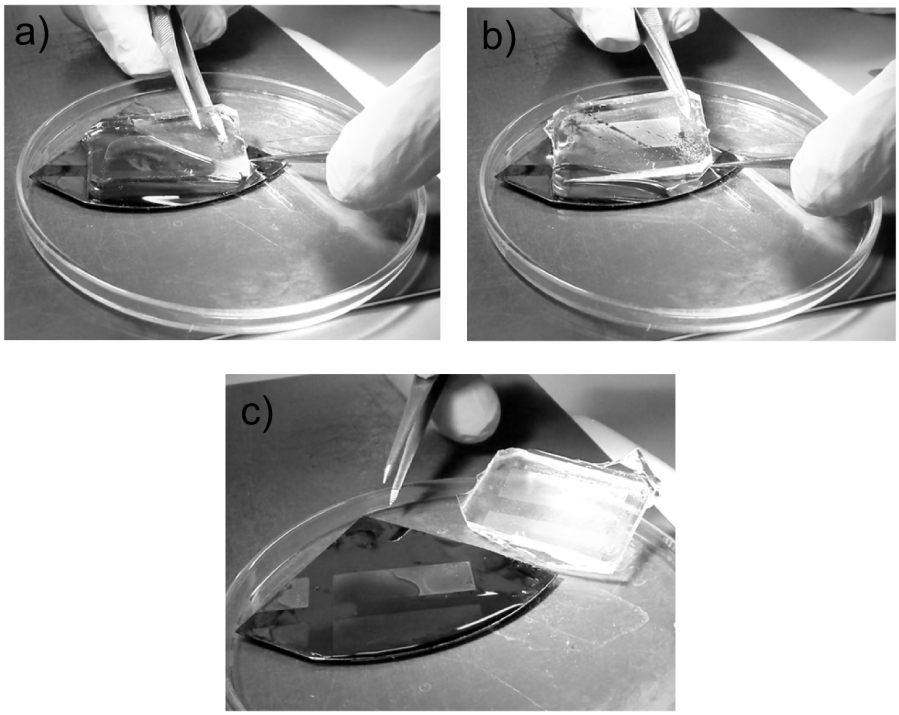

Figure A-9: *De-molding of the membrane adhered to the PDMS slab by dissolution of the photo-resist sacrificial layer on the mold. (a-b) An acetone lubricating layer is dispensed on the interface between the PDMS slab and the mold or alternatively the sandwich can be put inside a bath. Though, wetting and dissolution of photo-resist is automatic, aiding exposure of the sacrificial layer by de-lamination of the corners quickens the process. Also, for fur lift-off the slab must me manually removed from the mold with the use of tweezers.*
Critical: *Curving of the PDMS slab by peel-off should be avoided nor present as this is a sign of non-full wetting of the interface between membrane and mold. Considerable curvature of the slab while de-molding can promote cracking of the brittle dextran layer and therefore tears on the molded membrane. (c) Final lift-off of the PDMS slab from the mold is possible even without achieving full dissolution of the sacrificial layer.*
Note: *Once acetone has wet the interface, this should not be let dry as this will promote surface adhesion of the interfaces that can promote tear and difficult handling.*

- Successful de-molding results on a fully cured ≈ 10 μm 10:1 PDMS membrane adhered to the thick slab by a dextran layer interface and an intact pillar mold.
  Note: We have observed SU-8 molds were re-usable after thorough cleaning (acetone, ethanol and IPA rinsing) up to 5 times. The membrane and carrier slab must be thoroughly rinsed with acetone before posterior use.

- Rinse the PDMS slab sparsely for a minute, membrane-face side, with acetone and dispense on its surface leaving for ≈30 sec. Then, gently blow dry the acetone from the slab with nitrogen gun revealing a clearer PDMS membrane, see Fig. A-10.
  Note: Though long-term exposure of the membrane surface to acetone has revealed no negative effects on the membrane quality or affected its adhesion to the underlying dextran layer, it is not advised. Careful rinsing with acetone and blow drying is preferred to eliminate any surface contamination.

- Place the slab on a clean microscope slide for better posterior handling and store in a clean petri dish.

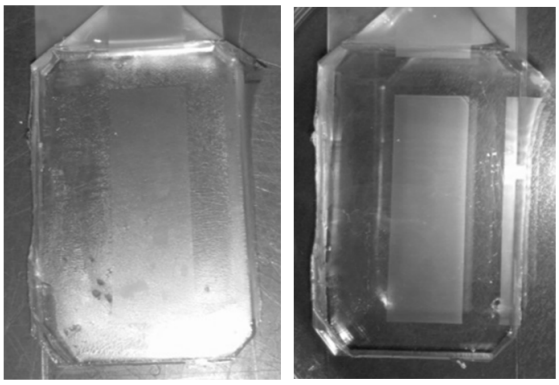

Figure A-10: *A final rinse with acetone; or bath immersion (≈ 30 sec), clears the membrane's surface so on the slab only the membrane molded area is not transparent. The slab and membrane can be compared before (left) and after acetone rinsing (right)*

Preparation and Sectioning of the PDMS membrane:
The clean membrane on the carrier can be either directly bonded to a device or cut into sections and then transferred depending on the size requirements of the final device. Though the uniform membrane film spawns entirely on the PDMS carrier (2.5 cm x 4 cm), only the molded region (1 cm x 3 cm) should be used; areas outside of this region were observed to be un-evenly thinner (<1 μm) and prone to break. The membrane and slab can be cut directly with a clean scalpel or razor blade; though, excessive handling promotes break of the membrane due to cracking of the dextran layer underneath. After cutting the membrane must be again cleaned before transfer.

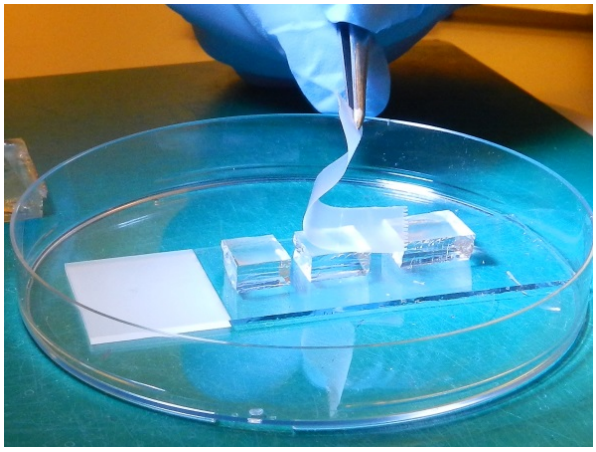

Figure A-11: *After dissection of the membrane and the carrier slab, the membrane surface must again be cleaned. This can be done as previously shown by acetone rinsing or by scotch-tape de-lamination.*
Note: *The membrane adhered to the carrier can be cleaned by careful de-lamination of particles with scotch tape; proving there is a firm adhesion between PDMS to dextran.*

- Treat the membrane and the corresponding final device by air plasma (20 W for 35 sec) and bring both surfaces onto conformal contact by careful tilting. A gently final push between the carrier holding the membrane against the device reduces any gaps due to discontinuities and ensures effective surface contact.
  Note: Always handle the membrane's surface by the PDMS slab carrier by using tweezers.

- Bring the set to incubation in an oven for 60 degC overnight to promote irreversible bonding. After this period the device and slab are brought to room temperature (≈15 min) before any manipulation is done.

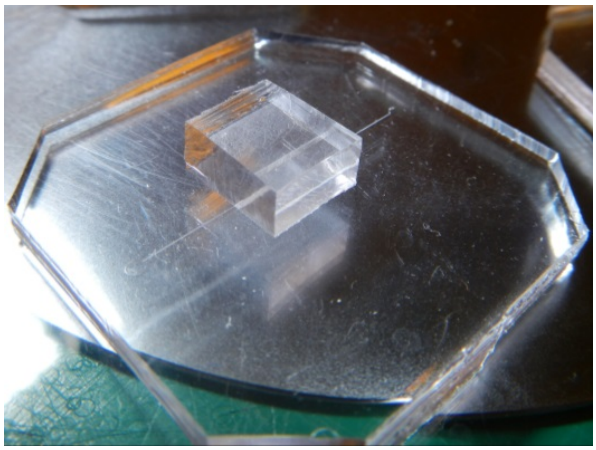

Figure A-12: *The membrane, still adhered to the PDMS slab carrier, is brought onto conformal contact with the final device after surface activation.*
Note: *We have observed that in the case of faulty positioning of the membrane, it is still possible to gently un-adhere it from the final device and re-position it without affecting final bonding strength.*
Note: *A short (30 sec) corona treatment also proved viable to promote irreversible bonding of the membrane to the final device. Neither air plasma nor corona treatment appeared to disrupt the underlying dextran layer or its ability to dissolve in water.*

- Release of the PDMS membrane from the carrier is done by first promoting water to filtrate into the thin dextran layer. Water is dispensed on the interface between PDMS carrier and device, and using the blunt tip of some tweezers, the surface of the device surrounding the area bonded to the membrane is locally pushed down. This motion aids to de-attach both surfaces and reveal the dextran layer which immediately is attacked by water.
  Note: A water with Tween (0.02 %) mixture (Tween 20, Calbiochem. Merk Milipore) aids wetting of PDMS.

- Once the whole perimeter is exposed to water by manual handling, the complete set is submerged in hot water bath (80-90 deg C) for at least 1 hour or until full lift-off is achieved. If correct lit-off occurs (long bath time $>$ 3 hr might be required), PMDS will automatically de-attach and float on the surface of water leaving behind a free standing

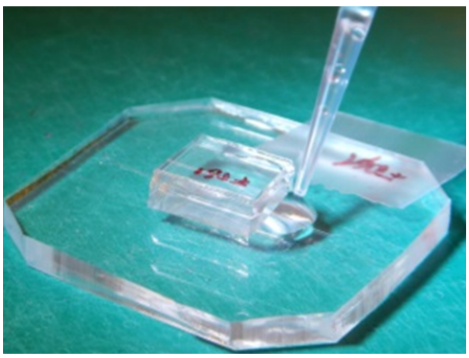

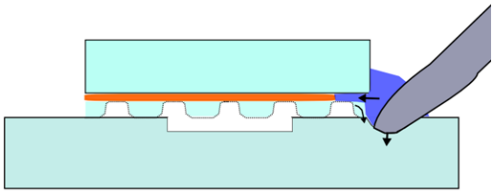

Figure A-13: *(a) Lift-off by dissolution of dextran in water is aided by mechanical exposure of the PDMS-dextran-PDMS. Due to hydrophobicity of PDMS, deposited water will not easily creep into the interface.*
Note: *To aid wetting, a mixture of water with Tween can be used instead of simple DI water. (b) The edges of the device can be pressed by a blunt tweezer tip to locally deform and promote exposure of dextran to water.*
Note: *Exposure of the membrane to water by manual handling should only be done at places where no sensible features; as free-standing membranes, are positioned due to possible break of the membrane.*

membrane irreversibly bonded on the device.
Critical: Agitation during release should be avoided as it promotes stretch and therefore possible tear and break of the membrane on free-standing position.

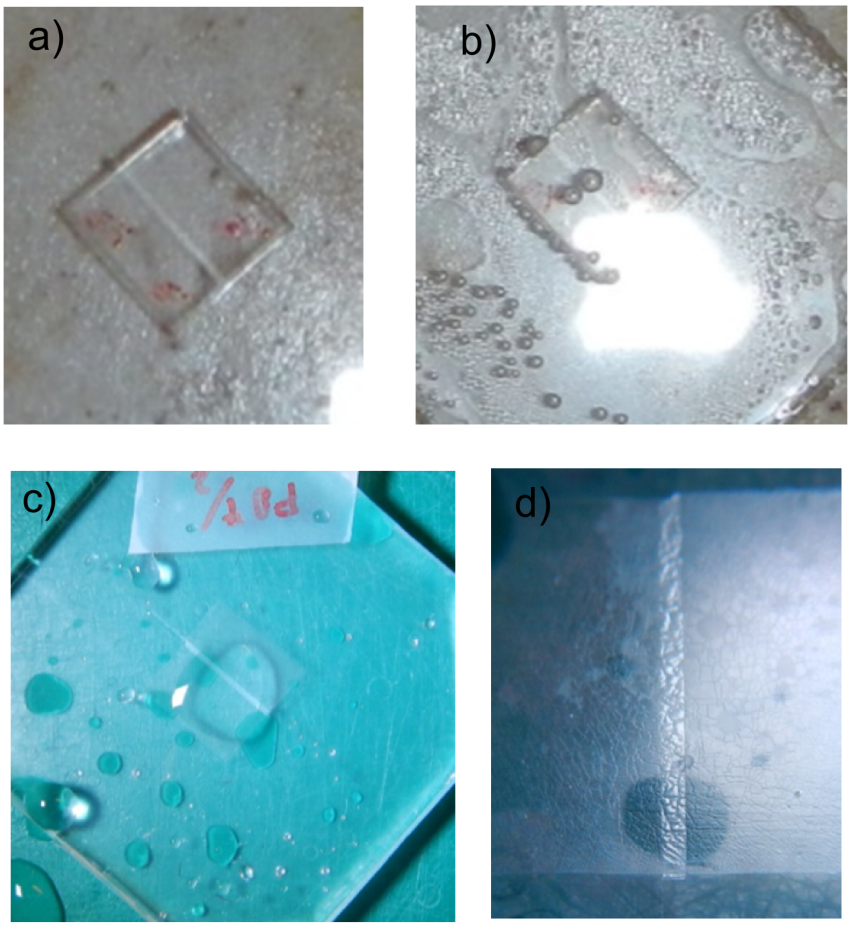

Figure A-14: *(a-b) Final lift-off occurs by immersion of the set in a warm water bath at 80-90 for approx 1-2 hr. During lift-off bubbles appear on the set and on the free standing membrane section. For long etching bath times, lift-off occurs automatically due to buoyancy of PDMS in water.*
Note: *Normally, lift-off occurs in a preferential direction and when the sensitive areas are already de-attached from the slab, the carrier slab can be manually de-bonded and the process stopped. (c-d) Final device with an irreversibly bonded free-standing membrane. (c) The membrane section shows hydrophilic characteristics and therefore it will remain wet after bringing it out of the water bath. (d) The membrane can be gently blown dried with nitrogen to displace the water trapped between the channel and membrane.*
Note: *After removal from the warm water bath PDMS shows translucency instead of transparency. We observed this effect disappears as the piece is dried in a couple of hours.*
Critical: *Any agitation of the bath or device before complete lift-off might promote micro-tears for large free-standing membrane sections.*

Appendix B

Membrane Fabrication Troubleshooting

B-1 Micro-tears

Micro tear of membranes during final lift-off.
Tearing of the membranes was observed only in the relatively large free-standing membranes (layed over circular 5:1 PDMS frames with a diameter 5 mm) prepared for cell characterization. Few of these defects (1-3) were observed for each sample (Figure B-1).

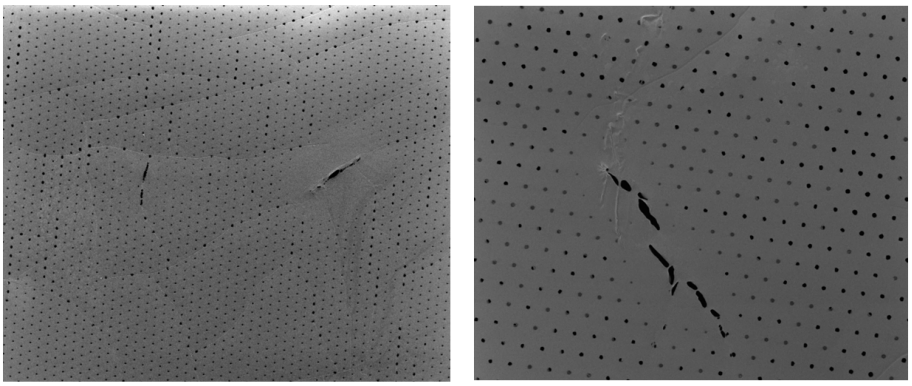

Figure B-1: *SEM images of two large free standing membranes (5 mm diameter) showing micro-tears. These micro-tears were the only present in the completeness of the membranes and have been observed to be small strips 100-200 μm long and 10-50 μm in width. This membranes were only present in large free-standing membranes and not in membranes on microfluidic channels (500 μm - 1000 μm width and several mm's large)*
Note: *Tears were observed to be promoted by agitation of the sets in the final lift-off process during immersion in a warm water bath.*

These defects are associated to agitation during lift-off of the thin compliant PDMS layer from dextran sacrificial layer. Longer etching times and avoiding any manual handling were observed to diminish or eliminate these defects.

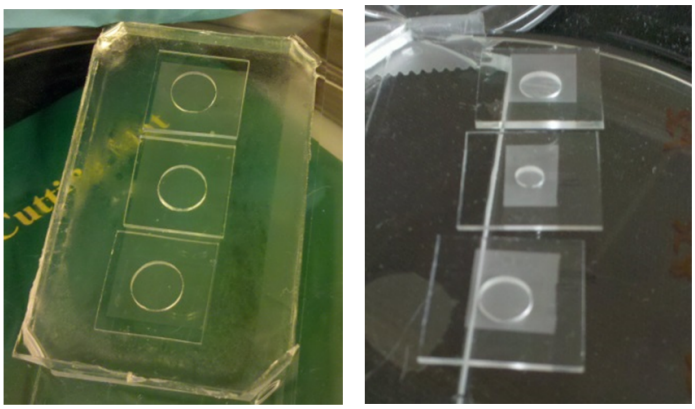

Figure B-2: *Large area free-standing membranes bonded to PDMS carrier before (left) and after release (right). Micro-tear defects are not assessable but only by SEM imaging.*

B-2 Cracks

Topographical defects on the membrane, similar to cracks (Figure B-3), were observed for manually aided membrane de-lamination and quick drying of the dextran deposited layer.

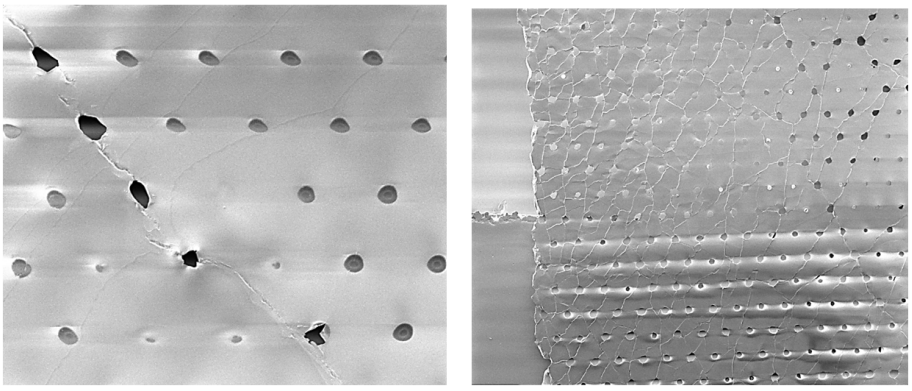

Figure B-3: *(a & b). SEM images of molded membranes showing cracking topography from cracked brittle sacrifical layer. (a) Detail of crack on membrane and topography details of substrate cracks. (b) Highly affected membrane surface due to mis-handling and wrong processing of substrate and dextran deposition.*

These molded cracks on the PDMS films were observed to be due to cracking of the underlying brittle dextran layer (Figure B-4). Wrinkling and cracking of the dextran layer can be attributed to intrinsic stresses induced during processing. On one side, intrinsic stresses on the layer can be attributed when deposition of the liquid layer occurs; this can be associated

to evaporation of water solvent in the dextran mixture. On the other hand, thermal stresses might also be present, this are due to difference of the film (dextran) and substrate (15:1 PDMS slab) coefficient of thermal expansion (CTE). The CTE of dextran has not been found and therefore thermal stresses cannot be further analyzed.

The observed defects could be associated to tensile stress; particularly since no buckling was observed and only cracks. Additionally, the PDMS substrate was observed to curve concave with respect to the dextran layer when this was not attached to the rigid microscope slide. The failure modes we can recognize are surface cracking, channeling, and substrate damage. Less surface cracking and therefore substrate damage was observed for relatively stiffer substrates (10:1 pdms), nevertheless these stiffer substrates were observed to promote other defects; such as clogging of the pores, therefore softer (15:1) PDMS substrates were used.

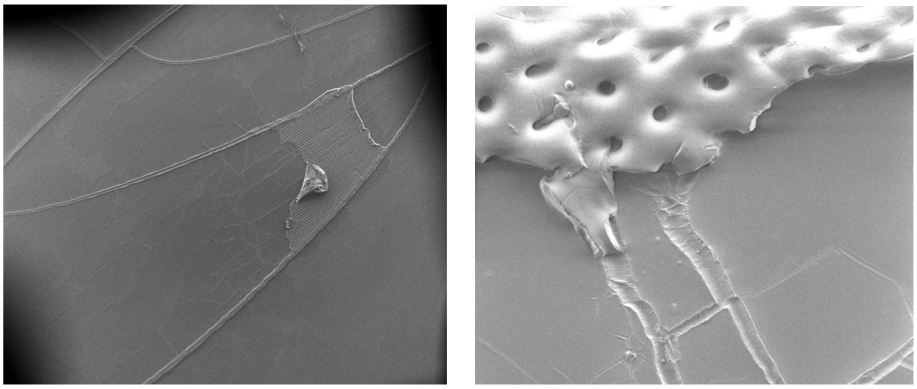

Figure B-4: *SEM images of cracks observed on the PDMS slab carrier substrate due to stresses for dextran deposition after membrane release. (left) Long-single, thick cracks were observed for deposition of dextran on 10:1 PDMS substrates by the method described in Chapter IV. (right) Detail of crack and membrane residue due to incomplete release from picture on the left.*

To eliminate this problem a long cool down to room temperature after complete evaporation of water in the coating layer was used. Though, in order to fully avoid any thermal stresses, either quick or non-thermal drying processes; such as nitrogen flow or vacuum-assisted water evaporation could be used. For the case of using nitrogen blown, non-uniformities in thickness of the spin-coated layer must be assessed.

B-3 Non-through Pores

Applying insufficient pressure when molding the membrane film results on formation of micro-wells instead of open pores. Though this effect cannot be assessed with bright field microscopy, it can be easily detected by SEM imaging when cutting a through section of a suspended membrane (Figure B-5).

Though the clamps were observed to generate fully open pores, they have consistently failed to generate a membrane with only open pores. Instead, some pores have been observed to have an ultra-thin PDMS layer clogging areas of the membrane (Figure B-6).

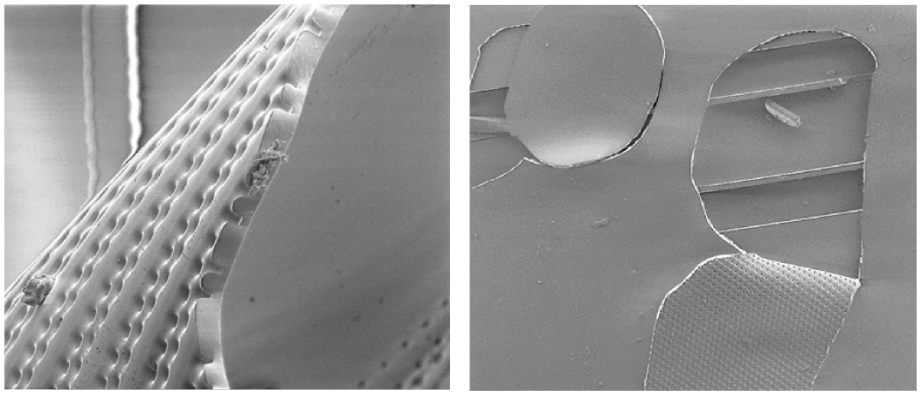

Figure B-5: *SEM images of non-porous membranes due to non sufficient molding pressure (300 gr weight used) and immmediate curing on hot plate. (left) Features of 7 μm pillars as micro-wells. (c) Non-porous PDMS membrane; dextran face siding up. A rupture was made with tweezers done to reveal the 10 μm micro-wells molded underneath.*
Note: *This problems were addressed by using a set of clamps instead of a weight and promoting longer curing times of the PDMS film at room temperature.*

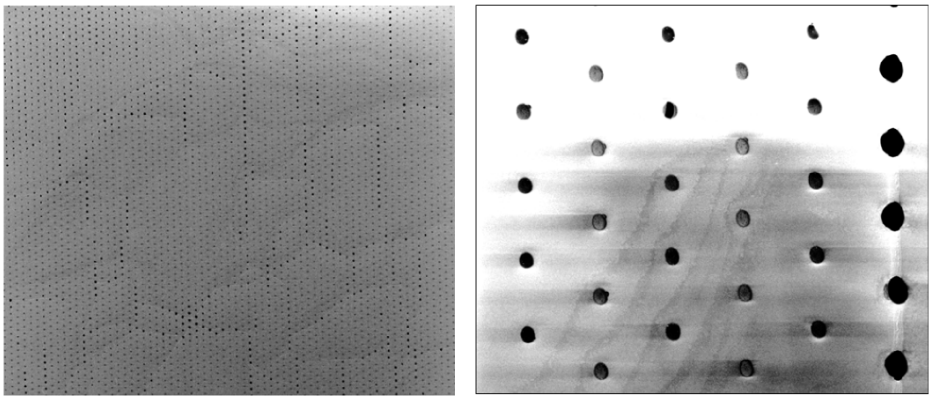

Figure B-6: *SEM images of membranes (10 μm pores) made from the reported fabricated process. (left) Non-through pores can be partially discerned by simple observation of large areas of the membrane. (right) Detail of through and non-through pores. The existence of an ultra thin layer can be assessed as those pores showing less contrast to the PDMS layer.*
Note: *Pores can be observed from either side of the membrane, in contrast to the previous micro-wells. The thickness of the ultra-thin PDMS membrane has not been assessed.*

B-4 Bulging and Stiction

Bulging of the membrane due to its own weight when laid free-standing over shallow channels was observed. The molded membranes (10um thickness and 10um pores), were observed to bulge when bonded to a 1.0 mm wide and 100 μm high PDMS microfluidic channel. The membranes were bonded and transferred to these channels as previously explained and bulging was observed at the end of the final lift-off step by water immersion when drying of water on the surface was done. Though it was observed that these collapsed portions of membrane did not irreversibly bonded to the bottom of the channels; by observing de-lamination of the

membrane by flowing of ethanol and acetone through the channel, the membrane did not free-stand and therefore using these wider channels was not possible for microfluidic testing.

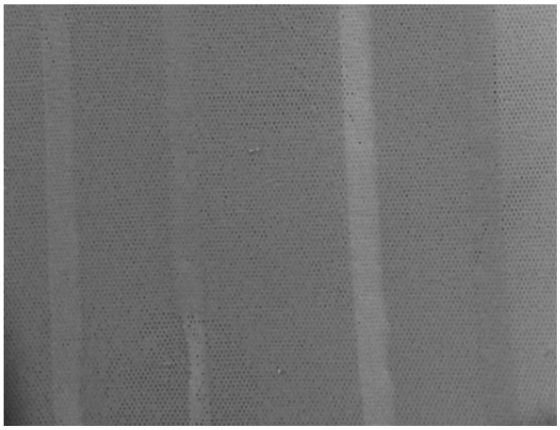

Figure B-7: *SEM image of 10 μm membrane irreversibly bonded onto parallel 1 mm width and 100 μm height PDMS microchannels. The membranes were observed to bulge and collapse on the bottom of the micro-channels.*

Additionally, the use of ethanol right after water lift-off created stiction problems. These stiction problem resulted in irreversible bonding of the PDMS membrane to the bottom of a microfluidic channel.

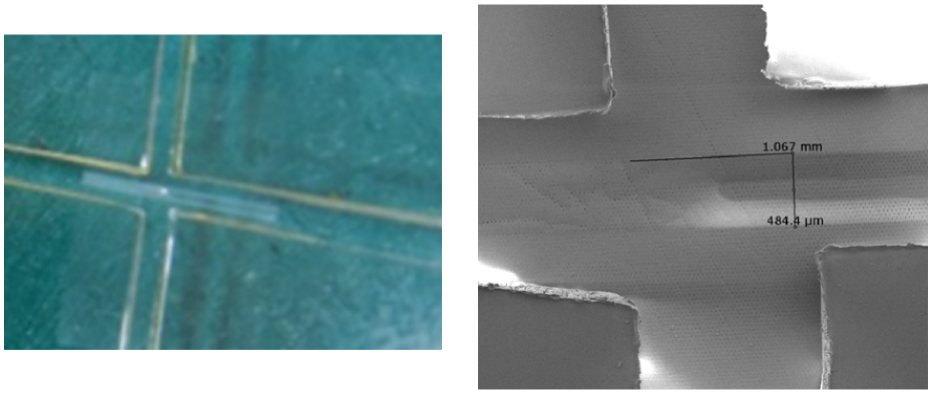

Figure B-8: *Stiction of a free-standing membrane on the bottom of 500 μm PDMS micro-channel due to ethanol evaporation. (left) Direct observation of collapsed membrane over channel. (b) SEM image of the collapsed and permanently bonded membrane on the PDMS micro-channel.*

B-5 Asymmetric pore profile

The profile of through and non-through pores on the molded membranes was observed to be asymmetric, on one side the membranes are fully flat and on the other the pores are observed to exhibit a smooth curvature (Figure B-9).

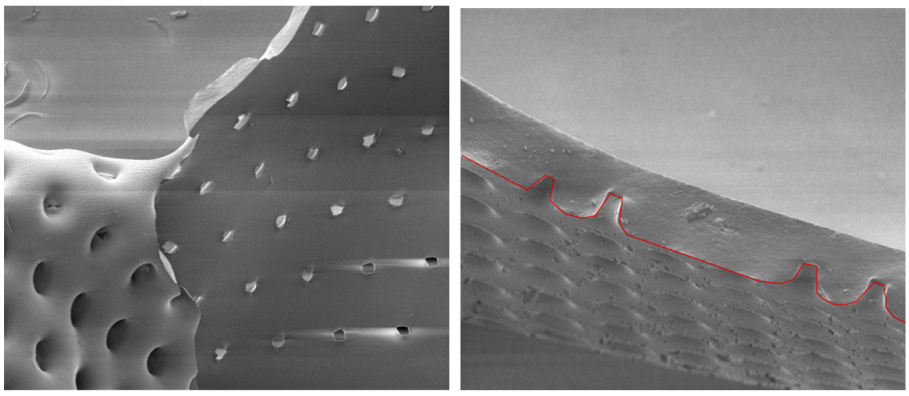

Figure B-9: *SEM image of fabricated membranes (10 μm diameter) showing an asymmetric pore profile. (a) It can be observed that on side (left) the membrane pores have a smooth profile transition, this side is molded against the coated pillar features. In contrast, the membrane side molded against the dextran layer (right) is flat, and the pores do not have a transition but instead have an ultra-thin residual PDMS rim. (b) The transverse cut of the non-porous membrane molded on the coated pillars shows the coating is non-conformal.*

The molding features were imaged with and without the lift-off (photo-resist) coating to determine the conformity of this layer which could result in the pore profile. The steep pillar mold profile is seen in Figure B-10a and b. The photoresist coating was deposited and spin coated as form a uniform layer of $\approx$ 1.0 um. Nevertheless, it can be observed that the coating is non-uniform next to the features (Figure B-10c and d). A meniscus can be observed in the concave corners which can be associated to hydrodynamic effect of the photoresist lubricating layer. This profile becomes the negative of the membrane, therefore the pore profile of the membranes are observed to be asymmetric and showing a smooth chamfer instead of steep edges of the pillar. In the valley between pillars, the coating was measured to be approximately 1.0 μm; the desired thickness, nevertheless the lateral coating thickness could not be assessed.

Though this transferred profile is not desirable and could be almost completely reduced by using an anti-stiction monolayer coating instead of an sacrifical layer, the form of the profile actually helps de-bonding of the membrane from the pillar mold and could be tuned by surface treatments and change of spin coating parameters.

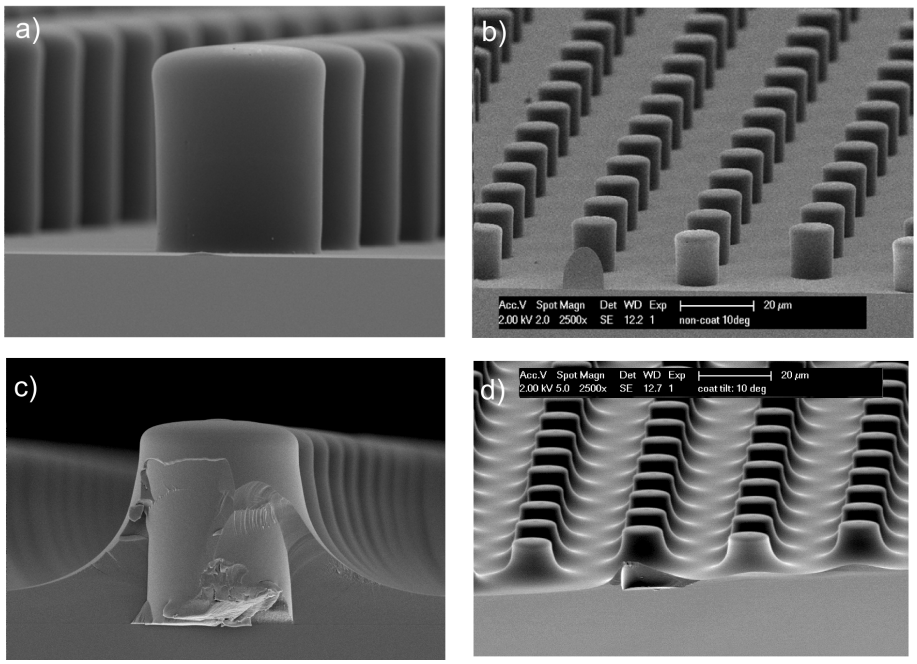

Figure B-10: *(a & b) SEM images of the SU-8 on silicon molds used to fabricate thin micro-porous PDMS membranes. (a) Detail on a single pillar. The pillar profile shows a small inverted tilt classic of negative photo-resists and a small aspect ratio. (b) Tilted perspective showing the pillar array distribution and homogeneity. (c & d) SEM images of the photo-resist spin coated layer on the SU-8 on silicon features used as molds to fabricate thin micro-porous PDMS membranes. (a) Tilted perspective showing the pillar array distribution and homogeneity of the photo-resist coating layer. The valley formed by the non-uniformity between pillars was measured to be approx 1 μm; which was the expected coating layer thickness. (c) Tilted perspective of a single coated pillar. (d) Detail on a coated pillar from a perpendicular view. The pillar profile shows photo-resist coating is highly non-conformal, though from the image the coating's thickness cannot be estimated but only with comparison with the non-coated pillar.*

Appendix C

SEM Imaging analysis

C-1 Pore Size

Pore size and form was observed to vary in all samples. As means to assess these variations, the SEM images of the free-standing membranes were analyzed using ImageJ (National Institutes of Health, Bethesda, MD). After proper scaling, cropping and threshold, the pores were analyzed as 'particles'. Individual estimation of pore areas are obtained and by assuming a circular profile, a pore diameter is calculated.

Analysis Procedure

- First, the images are scaled in ImageJ by drawing a line to match the image scale and the 'Set scale' function is used. Here the pixels are converted to the observed length scale embedded in the picture.
- Afterwards, the image is cropped so it only includes the features to be analyzed, the scale embedded in the image is also cropped-out.
- Then, the pores are highlighted by adjusting Brightness/Contrast such that the maximum is located at the peak (Figure C-1).
- The threshold of the image is set such that it is possible to discern between open and closed pores. Open pores normally appear to have a higher contrast to the membrane surface, in comparison to clogged pores (Figure C-2).
- Then, the function 'Process -> Binary -> convert to Mask' is used (Figure C-3).
- With the image as a binary, it is possible to use the 'Analyze Particles' option. Minimum and maximum particle size and roundness can be set to disregard defects from the image, e.g. un-complete pores imaged might be recognized as small particles.

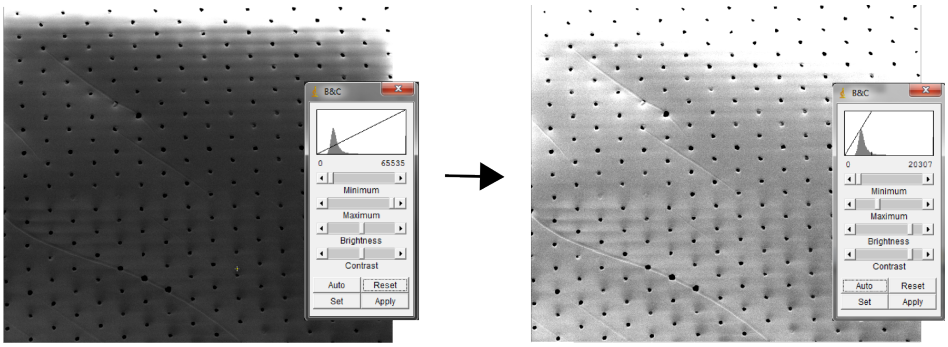

Figure C-1: *(left) Maximum limit of brightness and contrast of the SEM image is adjusted. (right) Individual pores are better recognized from the background of the membrane.*
Note: *The adjustment is done by subjective observation and thus it hasn't been automatized.*

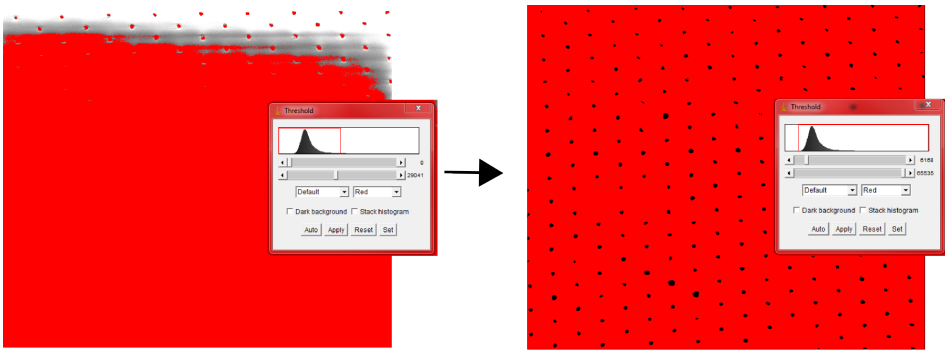

Figure C-2: *(left & right) Threshold is adjusted to discern between pores and background.*
Note: *The adjustment is done by subjective observation and thus it hasn't been automatized.*

- A dialog box gives the data generated from the analyzed particles, including the individual areas of the outlined pores (Figure C-3 right). Saving this sheet allows further processing.

- The data on the 'Area' column is processed to calculate a 'pore diameter' ($Area_{pore} = \pi(d/2)^2$).

- By truncating the calculate pore diameter for no decimals, histograms can be constructed in Matlab (Figure C-4).

- By using the histogram function that counts the quantity of pores of a given size 'bin-counts', the pore quantity, according to the pore size, is given as a normalized percentage of the total quantity of pores analyzed. In this way, many samples can be plotted together and a pore-size distribution can be observed for all the samples (Figure C-6).

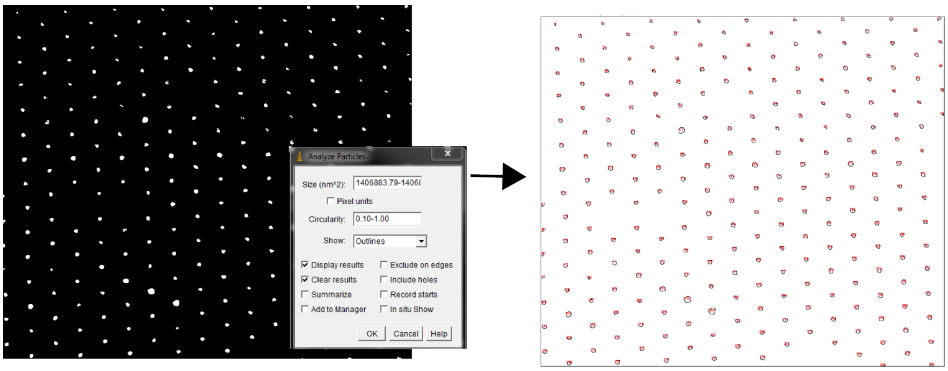

Figure C-3: *(left) The membrane image is made binary to leave uniquely the pore features to be distinguished for pore size quantization. The particle analysis function rectangle (shown superposing the binary membrane image) is adjusted by settling a minimum expected pore size (given in the scaled units) and a circularity (used to establish how circular is the pore expected to be). Marking the 'show outlines' tick helps identify the quantized pores from the previous image for correlation. (right) The quantized pores' outline is given in red. For every 'pore' analyzed the outline is given a number, this helps identify if the pore is quantized as unique feature; alternatively, as the pore density distribution is known, it can be known if defects such as partially clogged pores are being account as a unique pore or as openings through the ultra-thin clogging-membrane covering the pore. Together with the marked image, ImageJ provides a data-spreadsheet containing the quantified 'particle area'. Saving this information in a separate file allows further analysis of the obtained pore information.*
Note: *The adjustment is done by subjective observation and thus it hasn't been automatized.*

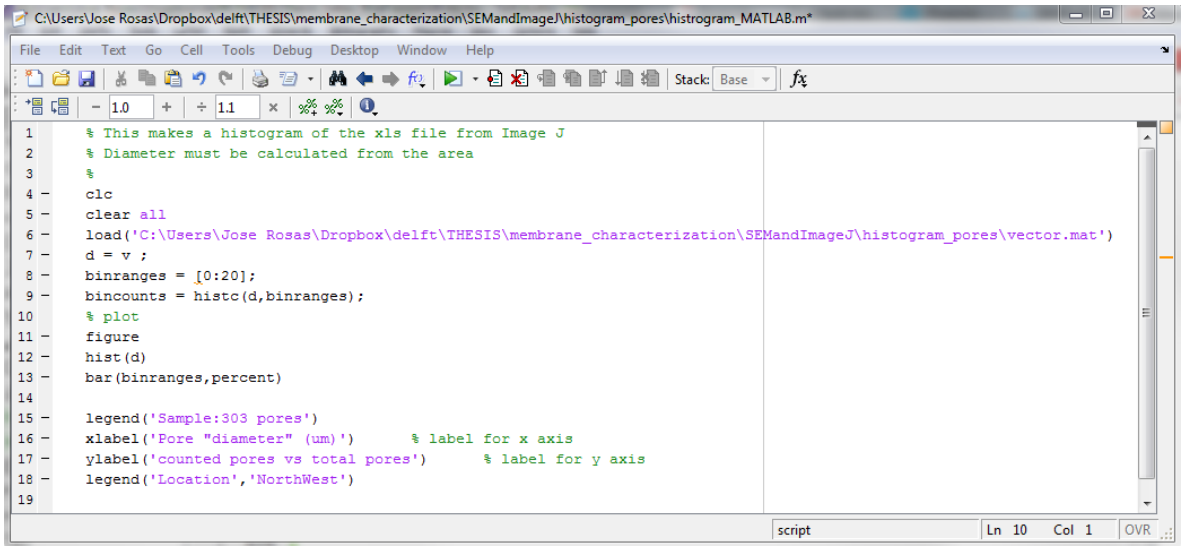

Figure C-4: *Histogram plotting code for individual pores implemented in Matlab.*

Results

Different samples analyzed reveal the average pore size derived from SEM observations is smaller than molded 10 μm objective. Since the membranes were always imaged from the side molded against the dextran layer, it can be inferred that the pore outlines analyzed with ImageJ contain the PDMS rim, thus partially clogging the pores.

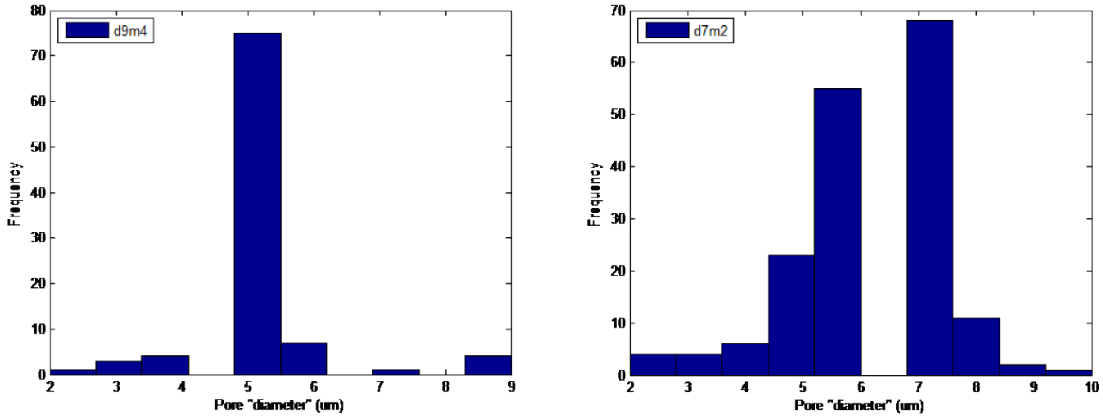

Figure C-5: *(left & right) Histrograms of calculated pore size for two different samples. Pore size distribution is observed to be different for both samples but in the same range (4-8um). These histograms were made by assuming a circular profile from the calculated pore-area of the ImageJ particle analysis. An equivalent circular diameter is calculated for the corresponding pore-area. This equivalent diameter is round-up for no decimals and a histogram is created in MatLab.*

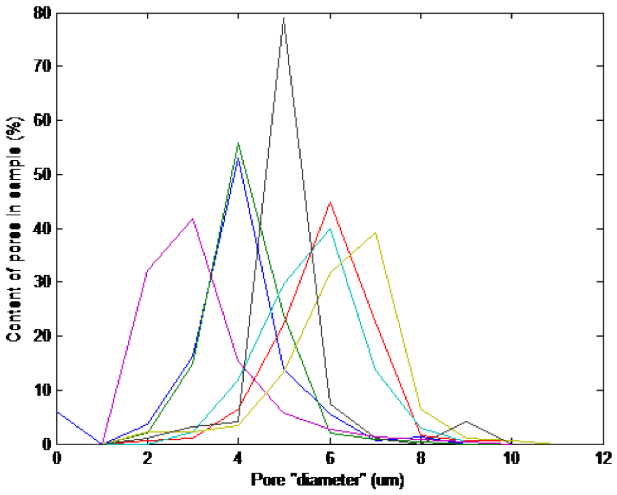

Figure C-6: *Histrogram showing percentual content of pores according to pore-size of various membranes. Individual histograms are shown with different line colors. The pore-size is observed to vary in distribution and size but within a common range (from approx 2 μm to 8 μm equivalent diameter). Individual pore-size content information was normalized to 100% for every sample to correct for porosity variations in the samples.*

Variations in pore size quantification

By using the strategy previously described to quantify pore size, the other side of the membrane; facing the molding features, was also analyzed to determine if the previously reported size is the same on both sides.

Result

By analyzing both sides of the membranes, two apparent pore sizes are obtained. On one side,

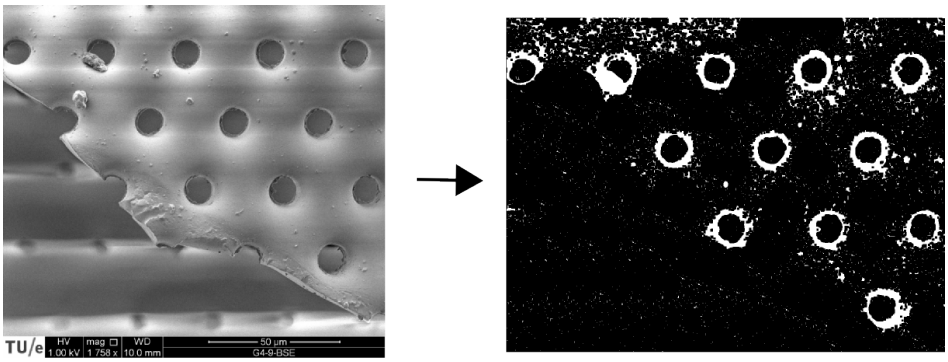

Figure C-7: *The profile of the pore observed from the side facing the mold shows size variations from the image analysis process used. (left) SEM image of porous membrane molded from 10 μm pillar features. The pore profile can be seen as an obscure rim surrounding the openings of the pores. (b) Same image after scaling, cropping, adjusting for brightness and contrast, threshold and binary transformation. The rims, which account for the pore profile, are seen in white. The outer perimeter is the pore diameter from the molding features, while the inner one is that as observed from the dextran molded facing side.*

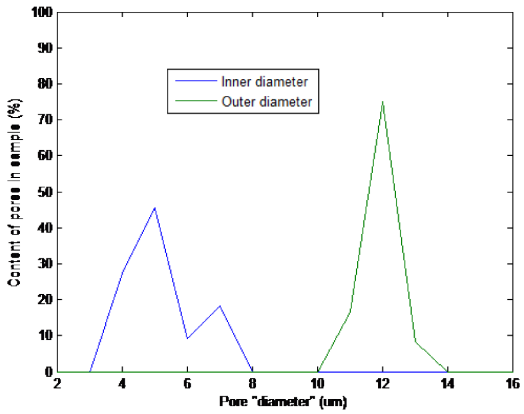

Figure C-8: *Histogram of FigC-7-b showing variations in calculated pore-size using the methodology previously described. In blue, the pore-size is calculated considering the inner-pore perimeter which is between 3 μm-8 μm; similarly as the previously analyzed samples. In green, the pore-size is calculated considering the outer-pore perimeter, showing a peak at 12 μm and spawning between 10 to 14 μm. Though the molded pore-size from the features is expected as 10 μm, the photo-resist coating layer; as observed in Fig.B-10, thickens the feature thus explaining the greater pore-size obtained.*

a big pore (10-12 μm) associated to the molding feature diameter, is correctly being molded on the membrane. On the other side, a small pore ($\approx$5 μm) associated to the existence of an excess PDMS rim, is associated to the observed potentially clogging ultra-thin PDMS layer over the pores. Overall, the pore profile, resembles a Gaussian function.

C-2 Porosity

Porosity (open pores vs. total pores) was assessed using a similar procedure to that used for analyzing the pore size of the SEM images.

- After proper scaling and cropping, the threshold of the image was tunned by subjective appreciation to 'distinguish' between *open* and *closed* pores.
- Once only the set of 'open' pores was viewed by thresholding, the pores are analyzed with the 'Analyze particles' function, which counts the selected pores.
- By repeating the thresholding step but now to cover all the pores observed, the analysis is repeated again to give a measure of the total pores molded on the membrane.

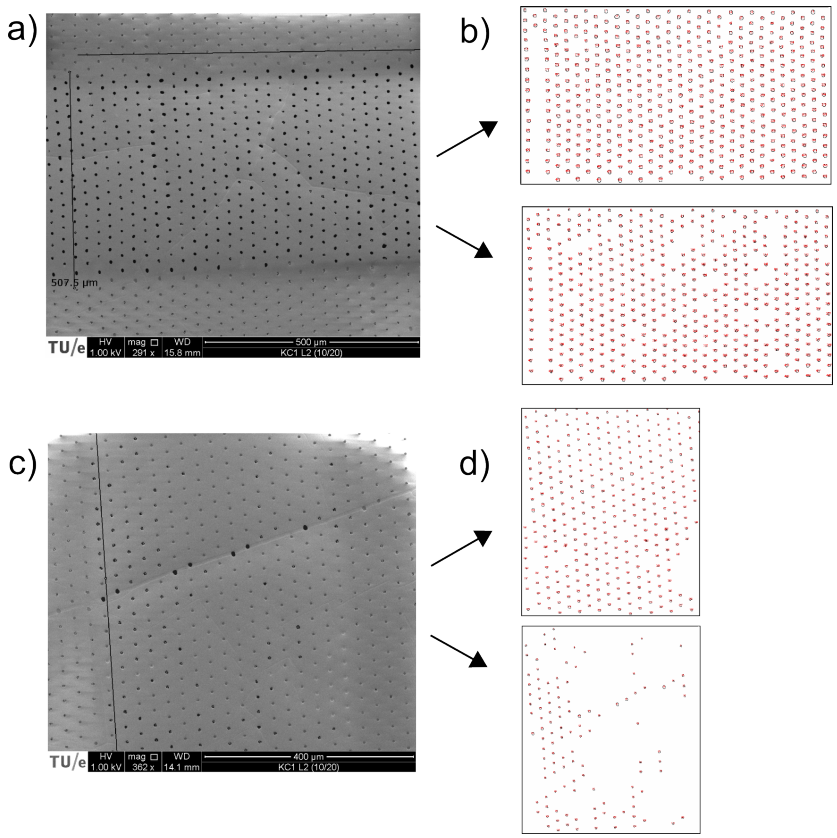

Figure C-9: *(a & c) SEM images of two samples showing apparent different porosity. (b) Total pores quantized (top) and open pores (bottom) of the membrane section in (a). The procedure shows apparent high porosity (≈ 90%). (d) Total pores quantized (top) and open pores (bottom) of the membrane section in (a). The procedure shows apparent low porosity (≈ 20%).*

Result

This analysis has shown plausibility to assess membrane porosity of small samples (< 1 mm x 1 mm). Only small areas in this range were able to be processed with the acquired SEM image quality. Porosity calculations by this method shows the membranes have different porosities.

	Porosity (# of open pores vs. # of molded pores)
D1M1	38.5 %
D2M2	88.2 %
D4M3	92.0 %
D5M4	84.0 %
D6M1	10.4 %
D7M2	92.3 %
D9M4	20.7 %

Table C-1: Porosity calculation results of seven different samples by SEM image analysis

Porosity is reported as the ratio between # of open pores vs. # of molded pores and was calculated to be either low < 40 % , or high > 80 %. Distribution of open vs clogged pores is observed to be random on the membrane and no correlation between samples was possible.

Appendix D

Fluid Characterization

D-1 Fluidic setup

The testing setup (Figure D-1), consists of a device made of two (10:1) PDMS microfluidic channels (100 μm height and 500 μm width) that sandwich the PDMS porous membrane (Figure D-2 right). Inlet and outlet access ports are punched only into one side of the PDMS device (diameter 1.2 mm punchers) thus allowing for bright field microscope inspection during the experiments. The device was connected by manual insertion of blunt needles at the inlet and outlet ports. At the inlet, two flows (Q1 & Q2) are well established by two syringe pumps, and at the outlets the tubing ends are suspended on recollecting vials. To begin the fluid experiments, the device is first filled entirely with a slow flow ($\approx$ 5 μl/min); this avoids trapping of air bubbles inside the channels.

D-2 Fabrication detail

Due to the thickness of the membrane sandwiched in between the channels, a small discontinuity, similar to a gap was observed at the rim of the membrane. Though this gap did not promote leakage during microfluidic experiments, the problem was minimized by gently pushing both sides together after surface oxidation and the addition of a small uniform weight ($\approx$ 300 gr) on the device during bonding incubation for $>$ 6hrs at 65 degC (Figure D-2 bottom).

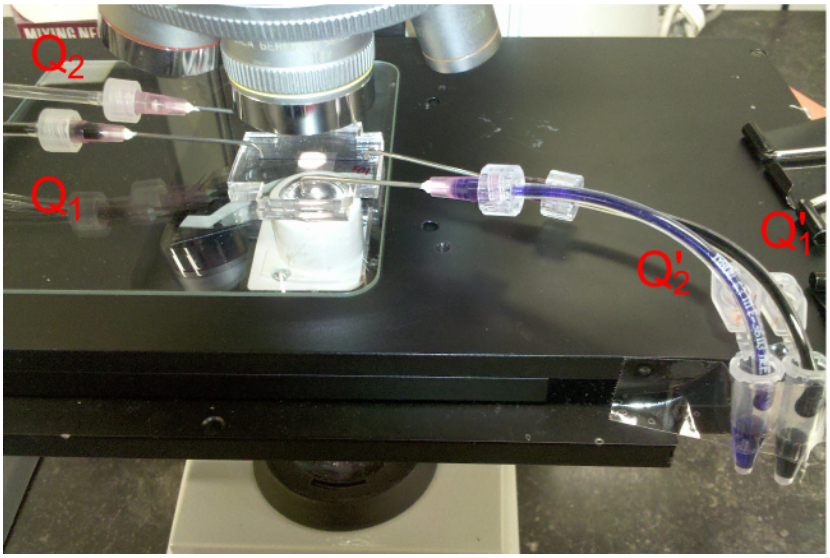

Figure D-1: *The fluid characterization setup consists of the device connected to input and output flows. Input flows ;Q1 and Q2, are imposed by a syringe pump and output flows are recollected in vials to quantize.*

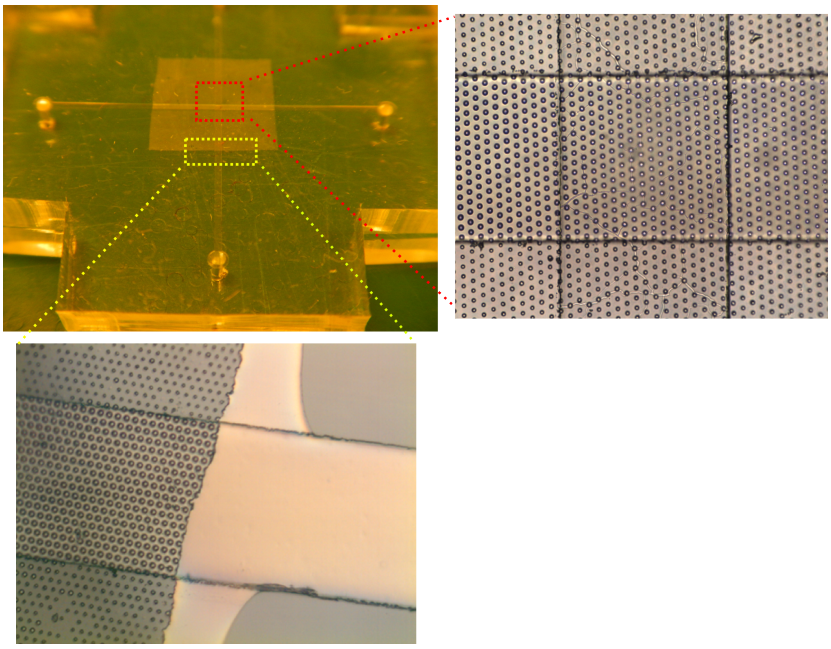

Figure D-2: *(a) Device with irreversibly bonded membrane used for fluidic characterization of porosity. (b) Bright-field micrograph of crossing section (500umX500um) between two channels in different planes separated by a free-standing membrane. The membrane shows no apparent deformations or defects, though determination of porosity is not possible by this method. (c) Bright-field micrograph of micro-gap observed at the interface between membrane and upper and lower device layers.*

D-3 Fluid circuit equivalent

The Hagen-Poiseuille equation $\nabla P = R \times Q$; that relates the pressure drop (∇P) within a fluid channel to the flow rate (Q) within and an equivalent fluidic resistance (R), was used to describe the flows within the criss-cross channels of the device and through the porous membrane. By using a syringe pump system, the flow profile establishing within the channels is expected to a parabolic profile with maximum in the center and no-slip condition on the walls. And to correctly account for this model, a laminar flow regime ($Re \approx< 1$) was established by setting the experimental flows within the channels < 15 μl/min.

A simple equivalent circuit model (Figure D-3) was used to predict the flow through the membrane in function of its porosity. To validate the model flow predictions as function of the porosity content, these can be compared to independently made calculations of porosity based in SEM images of the membranes on the fluid devices; as presented in Appendix C. The resistance of each section of the device (straight channels and pores of the membrane) are modeled to their equivalent fluidic resistance (based on Hagen-Poisseuille) and were calculated in Matlab. The calculated resistances and the established flows (Q1 & Q2) were inserted in the circuit model and simulated to obtain the output flows (Q1p & Q2p). Before all calculations all given values were changed to the metric system. The ratio of the calculated output flows (Q1p/Q2p) was graphed as a function of the input flows (Q1/Q2) to build axes on which to compare the fluidic experimental results.

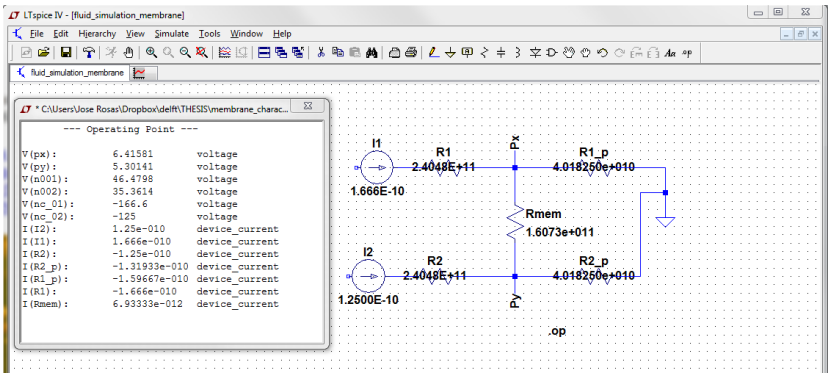

Figure D-3: *The circuit equivalent was built and simulated in LTspice. The model returns the correspondent current; flows, and voltages; pressures, from the modeling conditions imposed.*

Results: The results of both fluid experimental values and the circuit model calculations are graphed in Figure D-4. The results obtained by the flow recollection method only predict either highly or low porosity of the devices; similarly but not completely correlated to the SEM porosity calculations. The equivalent circuit model appears to be too simple, though partial correlation to the fluid experimental values can be observed. Additionally, the use of a dye to assess species transport through the membrane helps to observe actual flow through the membrane though only in a qualitative measure (Figure D-5).

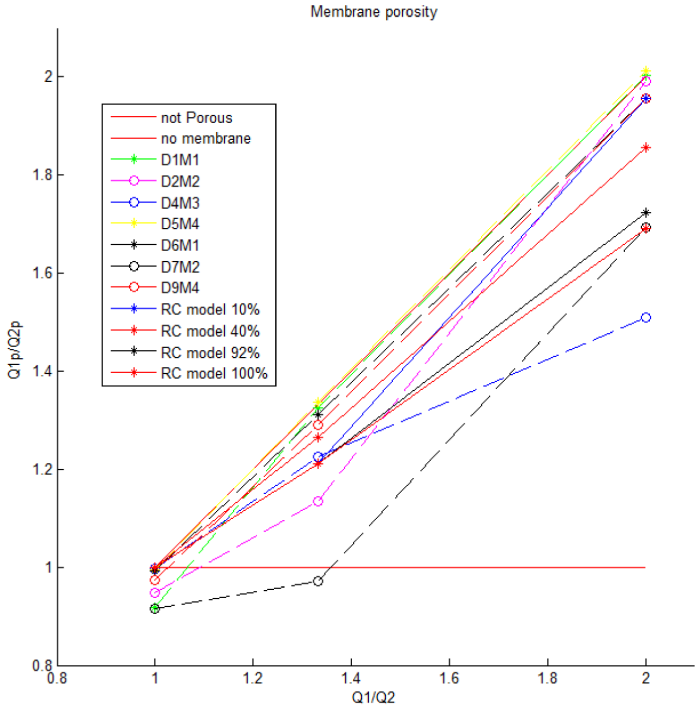

Figure D-4: *Fluid characterization results to assess porosity of the membrane. The hard red lines on the extremes denote the limiting cases of 'not porous membrane' (top) and 'no membrane' (bottom). The other hard lines, represent the calculated values from the equivalent circuit for 40 %, 92% and 100% of open pores. The dotted lines are the graphed experimental values obtained.*

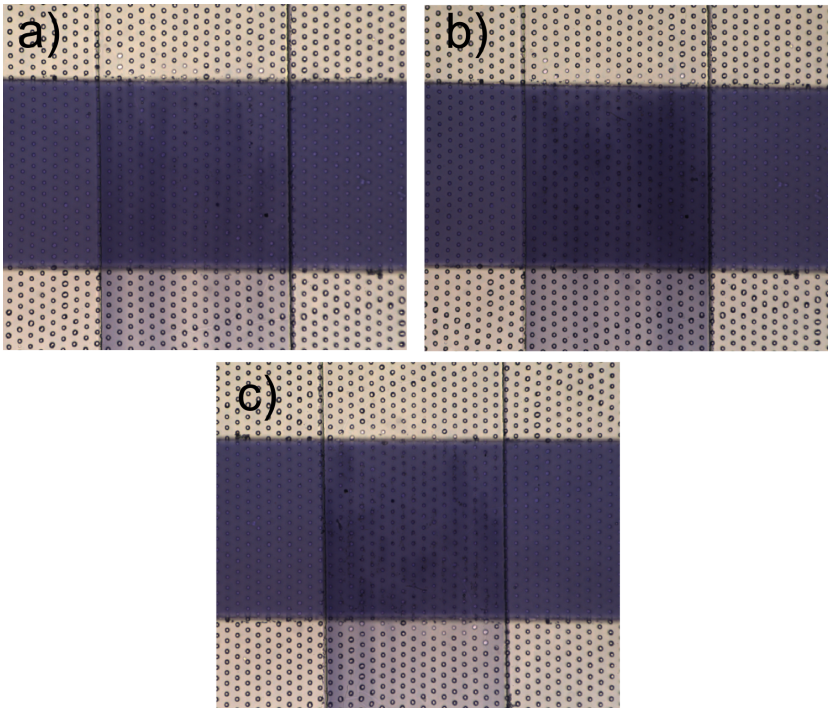

Figure D-5: *Micrographs of advective flow with dye passing through the membrane for different flow ranges during the fluid experiments, as means to assess porosity and leakage. (a) Equal flow rates; 10 μl each. (b) Dye channel (Q1) with a flow rate of 10 μl and clear channel 7.5 μl. (c) Dye channel (Q1), doubling the flow of the DI water channel; 10 μl vs. 5 μl respectively.*

Appendix E

Background on Cancer Metastasis and Cell culture

E-1 Physiological Background of cancer metastasis

E-1-1 Physiology of a solid tumor

A tumor is an abnormal growth of cells that reproduce indefinitely without an apparent purpose due to a malfunction of their genome. Once some of these gain the ability to spread, invade and promote growth of secondary tumors in other tissues, the tumor is considered malignant and called a cancer. Tumor cells are inherently different, depending on their environment of precedence these differences can be phenotypical; i.e. breast or intestine tumors exhibit different morphology in their microenvironment, but even within a tumor mass the differences can be genotypical; i.e. a cancer cell could be either associated to endothelial functions or instead posses stem cell abilities which are associated to invasion and growth of metastases in secondary sites [36]. A tumor is not composed uniquely of tumor cells but, in contrary, it is believed that more than 80% of its mass is composed of various kinds of cells and a biomatrix or extracellular matrix (ECM); that all-together is called stroma [4]. In addition, other structures such as blood vessels are known to grow into the tumor mass to bring nutrients. Within the tumor, a continuously mutating tumor cell niche grows while the stromal-cell population changes due to invasion from nearby tissue and permeating vessels. Furthermore, the ECM is continuously being remodeled and changing due to the interaction of all these agents within it. As a consequence, the tumor mass comprises a complex and dynamic bio-chemical and mechanical micro-environment that is believed to promote tumor progression towards a cancerous state.

E-1-2 Transition towards an invasive Cancerous Tumor

Metastasis is considered a process that occurs stepwise. First, tumor cells loose inter-adhesive properties to other cells and the ECM. Then, there is an increase in motility and invasive-

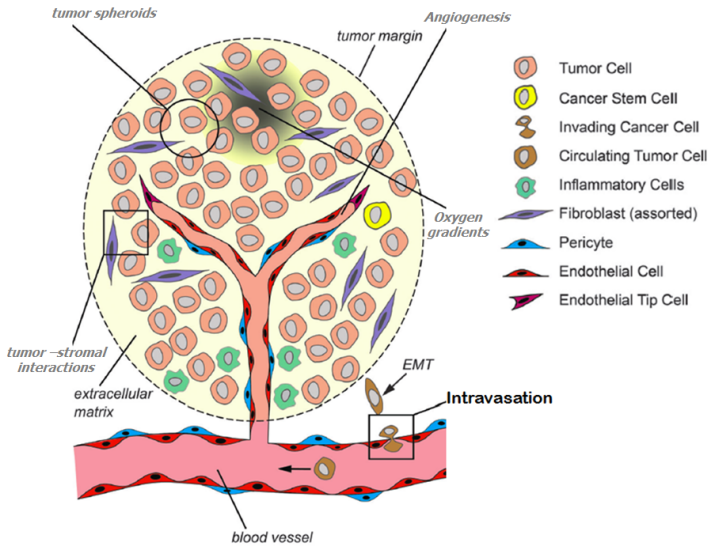

Figure E-1: *Illustration depicting the complex tumor microenvironment composed of tumor cells and stroma inside the ECM tumor mass. Various biochemical environments are created within the tumor as blood vessels and capillaries permeate the mass with nutrients. Additionally tumor and stromal cells together with the ECM continuously secrete and absorb soluble signals in a complex interplay that is hypothesized to promote cancer progression. Some of the main steps leading to metastasis are shown, such as EMT and intravasation of cancer cells into blood vessel. Image taken from [4].*

ness of these cells promoted by the bio-chemical and mechanical interplay with the micro-environment. The cells achieve entry and survival into the circulatory system (i.e. intravasation); or lymph nodes, promoted by bio-chemical and mechanical gradients. Finally, the cells exit into a new tissue (i.e. extravasation) and secondary tumor growth promotion occurs. Though many key changes have been observed, the inherent reasons for which each step occurs is still primary focus of research [6].

It is hypothesized that an *endothelial mesenchymal transition* (EMT) process transforms tumor cells and allows them to become invasive and colonize other organs. EMT changes the genotype of tumor cells such that their abilities are similar to those of cells responsible for angiogenesis. In this manner, the now "malignant tumor cell" (or cancer cell), is able to make its way out of the tumor mass, into and through a blood vessel and infiltrate in a secondary organ in which it will pursue to proliferate. Various signals and events affecting the tumor mass are known to promote EMT, such as: Metabolic stress (i.e. hypoxic conditions leading to acidic regions), mechanical stress (i.e. pressure and stretch due to cell excessive proliferation), immune responses (i.e. infiltration of white blood cells such as leukocytes and inflammatory recruited macrophages into the tumor mass), and accumulation of mutating cells. Nevertheless, the complex interplay of these factors that leads to metastasis is still an unresolved matter [9]. Despite many of these signals have been studied by independently, by observing characteristic changes of cells and their environment, it is the understanding of their interactions which is of most interest to provide clues on how to trigger and potentially stop tumor progression.

Mechanical changes of cells and ECM in a tumor

Relevant changes in mechanical characteristics of the tumor tissue and the interplay of forces during cancer progression has been observed and throughly reviewed in the literature [37, 38, 6, 39] It has been shown that breast tumor progression is accompanied by increased deposition and cross-linking of collagen type I (i.e. non-cellular structural protein component of the stroma) which results in tissue stiffening leading to amplification of bio-mechanical feedback [38]. Viscoelastic properties of living cells are modified by many factors in the 3D tissue, such as cell−cell interactions, effects of the vasculature and of the ECM. It has also become evident for the case of isolated cancer cells their hypersensitivity to substrate stiffness. Furthermore, stroma-cells show also mechanical sensitivity and changes due to interplay with their micro-environment[3]. While isolated cancer cells become increasingly compliant during tumor progression, breast, lung and brain tissue stiffens for an activated cancer state ; the elastic modulus of breast tissue for benign and cancerous state is 2 kPa to 12 kPa respectively. Whereas, stromal cells involved change independently; epithelial cells soften from 2 kPa to 0.4 kPa, fibroblasts stiffen 0.4 kPa to 1 kPa as so macrophages from 1.5 kPa to 0.5 kPa [38].

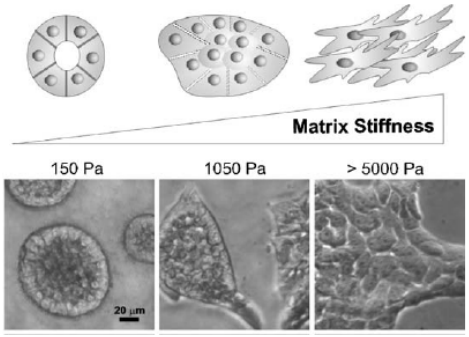

Figure E-2: *Change in morphology of mammary epithelial cells for increasing substrate stiffness. For soft substrates a defined structure is retained and held together by intra-cellular bonds. Higher stiffness disrupts these bonds and elongated, non-structured cell distributions are observed; these morphologies are associated to highly mobile, invasive and stem-property-like cells. Image taken from [39].*

Intravasation via transendothelial migration (TEM)

Intravasation refers to the process in which cancer cells migrate through the progressively stiffened tumor tissue (composed of a basement membrane and the interstitial ECM) directed by bio-chemical gradients and eventually penetrate into the blood-stream or lymphatic vessels [38]. In the case of intravasation into a blood-vessel, *trans-endothelial-migration* (TEM) occurs In this process, the metastatic cell gains entrance into the circulatory system by breaking apart the lining endothelial-cell layer that compose the blood-vessel. First, the basement membrane surrounding the tumor is broken down and migration occurs through the ECM-filled interstitial space. Eventually, at the interface with the blood vessel, the inter-cellular endothelial bonds (Vecadherin) holding the cells together are broken, thus disrupting the *tunica intima* structure of the vessel. Whether the cancer cell disrupts these bonds mechanically or if other additional biological mechanisms are involved remains not fully known[40]. For the case of cancer cell invasion into the lymphatic system no such endothelial-cell layer; neither a basement membrane, is present to transverse[41].

Stimulated migration of cells by a gradient of a chemo-attractant is a central part of physi-

ological processes such as wound repair and metastasis[42]. During cancer cell intravasation and extravasation, these signaling molecules are brought by the capillary system into the tumor mass or released by target organs and are proposed to guide migration [43]. Additionally, various mechanical forces (e.g. interstitial compression, fluidic pressure and associated shear-stresses) together with non-homogenous stiffness profiles of the ECM are known to influence the rate and direction of tumor cell migration[38]. Guided migration due to a stiffness gradient is called "durotaxis" and it is of particular interest to understand the gradual stiffening of the tumor tissue during cancer progression and help indicate the migration path of cancer cells[38].

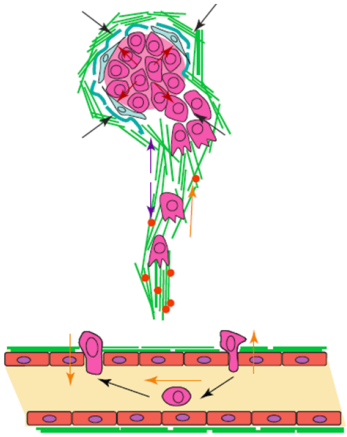

Figure E-3: *Scheme depicting migration and invasive behavior of cancer cells by relevant bio-chemical stimulation. After escaping the solid tumor and transversing the ECM, the cancer cell enters the blood stream by squeezing through a cell monolayer barrier part of a blood vessel. The cancer cell will travel through the blood-stream until finding a spot to escape this blood vessel to further on invade an organ where to establish a secondary tumor. Image taken from [38]*

E-1-3 Mimicking cancer on a chip: The Smallest Functinal Unit

The difficulty to understand the complex bio-chemical and mechanical interactions controling invasive propensity of cancer cells has been largely limited by the challenge of studying their micro-environment under physiological conditions[44]. To replicate this micro-environment; as an organ-on-chip, it is of most importance to determine the most essential biological, chemical and mechanical components that enable tumor cells to become invasive; undergo EMT, and further-on achieve TEM. EMT is hypothesized to initiate at the border between the tumor and normal tissue due to the greater likelihood of encountering there known EMT inducing factors [36]. To narrow the micro-environment size of this tissue-border, other physiological considerations such as the diffusion limit length of oxygen and nutrients provided by the permeating blood vessels can be considered. The diffusion limit of oxygen in tissue is in the range of $100 - 200\mu m$ [9] and cells located further away from this distance are not able to survive. Furthermore, non-correctly irrigated tumors cannot grow and eventually metastasize. Considering this size range, the geometry of a microfluidic chip can be made as to mimic the interface between the tumor mass and a blood-vessel in which EMT and TEM could be observed and studied.

E-2 Cell culturing Background

Conventional cell culturing refers to laying cells within a medium on plastic plates or wells. Regulation of the culture environment within is static, since oxygen, humidity and temperature conditions are kept constant inside an incubator. For inspection, proper optical characteristics and design characteristic of the plates are desired so that microscope technologies such as confocal and fluorescence microscopy are used. In common standard cell cultivation practice, the surfaces on which cells are seeded are not prepared with any specific ECM coating. These coatings provide the cells with a more physiologically relevant growth substrate. The coating choice corresponds to the environment desired to replicate and the used substrate, e.g. common coatings used for silicone-elastomeric substrates are fibronectin, collagen or matrigel[3].

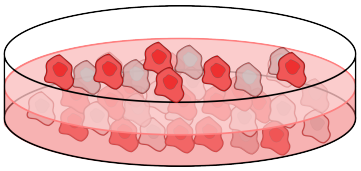

Figure E-4: *Cells are deposited on a glass or plastic dish, they are immersed within a medium that contains nutrients and factors that establish a suitable micro-environment that allow cells to grow.*

E-2-1 2D vs. 3D cell cultures

When seeding cells on a flat substrate, these attach to the container's bottom and proliferate to form a 2D cell monolayer. In-vivo, a *basement membrane* (BM); a tightly woven flat fiber substrate which promotes adhesion of cells [45], normally provides the support for 2D cell monolayers. A BM coating helps recapitulate some of the in-vivo cellular features with layed in-vitro flat substrates. Normally, after cells attach to the coated or uncoated substrate they deposit their own matrix. Eventually, this deposited matrix provide cells the closest physiological environment; though it must be considered that its characteristics and deposition are known to be dependent on the micro-environment provided as well as dynamic stimuli such as stretch and fluid shear-stress [3]. For the case of standard cell cultures providing these signals is limited. Alternatively, microfluidic platforms have proven particularly suitable to deliver precise, controllable and selective stimulation to cell cultures, thus achieving greater confluence, tighter inter-cellular junctions or gene expression for 2D cell cultures.

In order to mimic better the in-vivo physiological micro-environment, culturing of cells from rigid coated plain materials to soft and gel-like scaffolds has shown to provide cells a 3D structure in which these can bind and grow into a more relevant in-vitro culture. Cells are known to behave differently if cultured in a 2D or 3D fashion and these changes affect not only cell function but primary gene expression and epigenetic traits [3]. It is recognized, for example, that anti-cancer drugs act differently on cell-culture models when these are grown in a 3D like ECM medium than on a conventional 2D substrate [7]. Due to this, the use 3D cultures with materials such as alginate, gelatin and collagen have become tendency for integrating and developing new physiologically realistic micro-environments; particularly in microfluidic devices [46].

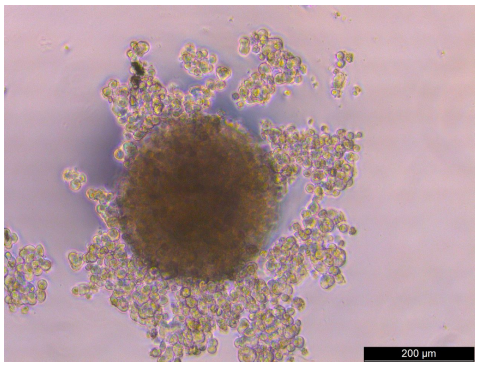

Figure E-5: *Micrograph image of a 3D cell culture of MDA-MB-231 breast cancer cells in collagen supplemented matrigel, it can be seen the cell morphology is cluster-like; called an organoid.*

Cell co-culture

Multiple cell culture models are traditionally achieved by (i) placing one cell type in direct physical contact to the second cell type; in which one type forms a monolayer of underlying 'feeder' cells, or (ii) using a porous membrane to compartmentalize each cell type while allowing soluble signaling factors through. Additionally relevant is that when using a membrane, decoupling of biochemical and mechanical signals is prevented, as in contrast when having direct inter-cellular contact.

When using membranes, these are traditionally clamped in a static assays where little control over the micro-environment is possible. Due to these limitations there is an increased interest of using membranes in microfluidic systems in which spatial control of cells and of fluid flow is improved [4]. Thin porous membranes layed over microfluidic channels (e.g. microfabricated PDMS or commercialy available PC and PET membranes) have been proven to work as bi-culture supports of cell monolayers grown on each side after proper treatment of the membrane with a relevant coating as fibronectin or collagen [2, 44, 47].

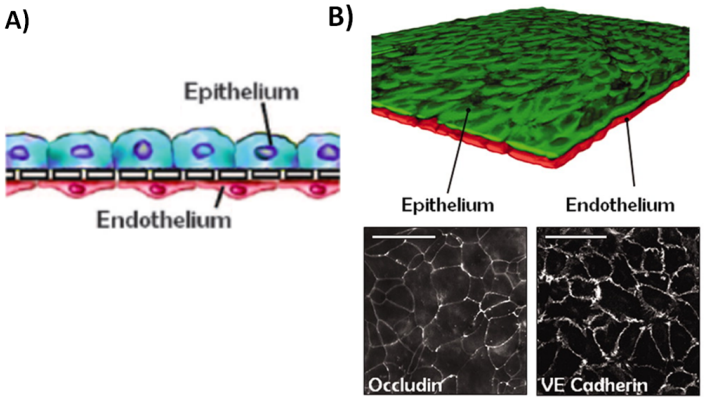

Figure E-6: *(A) Co-culture scheme of two cell monolayers (human alveolar epithelial cells and microvascular endothelial cells) separated by a thin ($10\mu m$) porous PDMS membrane. (B) The co-culture is stained for optical visualization and assessment of confluence of both cell monolayers (Scale bar 50 mm). Images taken from [2].*

E-2-2 Cell Migration Assays

Chemotaxis is the process of active migration of cells due to a concentration gradient of a relevant chemo-attractant. Migratory and invasive properties of cells have been widely studied in specially designed assays that permit stimulation of cells by chemical signals. The most commonly used migration assay design is the *Boyden chamber*; which has been key for the study of cell migration[46], this set-up is a static assay that consists of two chambers separated by a thin porous membrane (Figure E-7). This assay is made by thermo-molding making it cost-effective and biologically compatible. The commercial membranes integrated in these are normally made of PET and PC with different pore sizes and porosities.

Depending on the size of the pores, the effect of a chemical gradient on a separate cell chamber or migration activity of cells through the membrane can be studied. While for narrow pores (0.1-0.5 μm) particle diffusion through the membrane is possible, to allow movement of cells bigger pore sizes (3.0-10 μm) are needed, depending on the cell type. A drawback of this platform is that the gradient created by simple diffusion is linear and transient, therefore there is little control on the stimulation provided to the cells. Furthermore, it must be taken into account the decay time of the gradient in comparison to cell motility speed. Quick decaying gradients might not offer long experimental times to allow for sufficient stimulation of slow cells; i.e. cancer cell migration speed is reported to be relatively slow to that of other cells like neutrophils (1 $\mu m/min$ and 10 $\mu m/min$ respectively) [43].

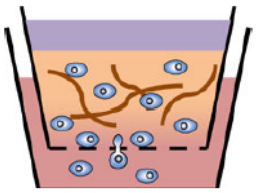

Figure E-7: *Scheme showing Boyden chamber assay for possible migration cells within a 3D medium due to chemotaxis. Standard cell migration tests are made in these assays, though several drawbacks have led to the use of other micro-fabricated assays. In particular, the little control of the stimulation provided to the cells and the limited microscope compatibility of the translucent PET and PC membranes. Image taken from [46].*

Discrepancies of the migration behavior and motility mechanisms of cells from 2D to 3D cultures have changed the focus to adopt the latter that better represents the in-vivo micro-environment [45]. Though 3D migration can be evaluated on a Boyden-chamber assay; by embedding cells in a 3D matrix, the additional limitations of this platform have boosted the development of alternative specially designed microfabricated platforms. In these devices precise control of the chemical and physical micro-environment can help resemble the in-vivo physiology while allowing real-time optical visualization and improved quantification of chemical and physical signals of interest for the study of cell culture progression[48].

E-2-3 Chemotaxis of cancer cells

Cell invasion is a complex process which requires migration of cells by making their way through an ECM or BM that act as physical barriers. Migration through these is achieved

by the cell attacking it either biochemically or physically; while biochemical signals secreted by the cell help degrade the barrier, physical disruption of the bonds holding these barriers together could also be exerted by the invading cell [29]. Henceforth understanding the ground mechanisms of cell invasion is of key relevance to study processes and progress of diseases involving cell migration.

Cancer cell invasion in metastasis could potentially be recreated and studied in a migration assay by building a relevant micro-environment. Several authors have studied distinct aspects of this process for different models; such as migration through porous membranes, gels and endothelial cell monolayers. Of particular interest for this project is the study of breast cancer, henceforth the models will be constructed for commonly used invasive and non-invasive breast cancer cell lines MDA-MB-231 and MCF7 respectively. A very complete review on relevant chemo-attractants to different aspects of tumor progression, growth, angiogenesis, intravasation and extravasation is presented in [49]. In particular, two chemo-attractants have been previously used to study and promote cancer cell migration.

Fetal Bovine Serum (FBS) as chemo-attractant

FBS is a common supplement in growth medium for cell culture, nevertheless it has been shown that by creating a FBS gradient in the cell culture, cells will undergo chemotaxis to the higher concentration region. It is reported that by using 20% FBS in medium as chemo-attractant (10% used in general medium) MDA-MB-231 cells migrated; migration was quantified at $\approx 7\mu m/hr$, through matrigel coated microgaps ($15\mu m$) in a microfluidic device. The gradient created in these gaps was maintained by refreshing the medium in specially designed reservoirs [28].

Endothelial Growth Factor (EGF) as chemoattractant

In the context of a metastatic tumor, EGF is produced by tumor invading macrophages and is associated with inducing aggressiveness and migration of cancer cells [49]. It has been reported that MDA-MB-231 cells seeded in a 3D ECM (matrigel w/ 2.5 mg/ml collagen type 1) in 10% FBS supplemented serum were seen to migrate through an endothelial monolayer (HUVEC) both in presence of macrophages (RAW264.7) and an EGF gradient[50]. Another study showed EGF induced migration of MDA-MB-231 cells at different concentrations (25-50 ng/ml) in a 2D fluidic configuration; migration rate is reported as $0.9\mu m/min$ and $0.5\mu m/min$ with and without stimulation. In this study it is observed gradient steepness is more relevant for inducing migration rather than higher concentrations; linear gradients did not promote migration. Appropriate coating of the surface also proved to be relevant as an adequate (2 μg/ml) collaged IV coating was most effective to promote faster and longer cell displacement [43] than higher and lower concentrations. EGF has also shown to increase invasiveness of MCF-7 cells as it was observed in another study in which a gradient was created by diffusion brought by two perfusion flows between a 3D gel composed of basement membrane extract (BME) with embedded cells. BME has similar components and characteristics to matrigel and contains many ECM-like components[51].

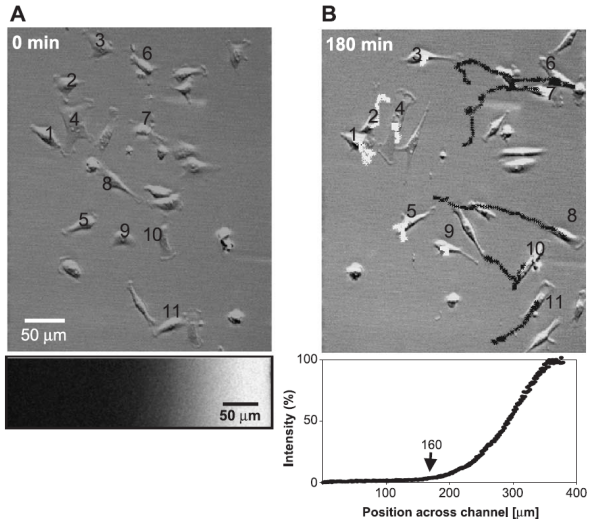

Figure E-8: *Micrographs from an inverted microscope setup showing MDA-MB-231 cancer cell 2D migration. The cells are observed to have an elongated morphology. A) Cells on the coated surface and a grayscale depiction of the gradient intensity at the beginning of the experiment. B) After 3 hrs only the cells on the steeper region of the gradient show migration towards a greater concentration region. Images taken from [43].*

Appendix F

Cell Characterization[1]

Membrane on PDMS carrier for cell experiments
Membranes were incorporated into a static migration assay composed of two stacked fluid-containing compartments separated by the porous membrane, resembling that of a commercial Transwell insert. The carrier rim consist of a 1 cm x 1 cm $\approx$ 700 μm uniform layer made by casting 5:1 mixed and degassed PDMS on a silicon flat substrate. A hole of 5 mm was punched in the center of the rim and then cleaned by rinsing with ethanol and dried with a nitrogen blow gun. Once permanently bonding them to the membranes by treating both with an air plasma and posterior incubation at 65 degC for 6 hrs, final detachment was done by immersion in a warm water bath. After successful detachment, the membranes were rinsed again by repeated dipping in a beaker with room temperature DI water.

Figure F-1: *Membrane on PDMS carrier used for migration and cell attatchement experiments.*

Cell adhesion
Adhesion of cells to the membranes was assessed by seeding MDA-MB-231 cells on the coated

[1]Cell seeding and migrations experiments were carried on at Philips Research, by Tom van Gijsel

membranes and inspecting their degree of confluence. First, the membranes were sterilize with isopropanol alcohol. Then, a 10 ng/ml fibronectin in phosphate buffered saline (PBS) coating was applied for 1 hour at 37 degC. The cells were then seeded and let to adhere to the fibronectin proteins for $\approx$ 1 hr. After that, 1 ml of medium was applied to avoid cells from washing off.

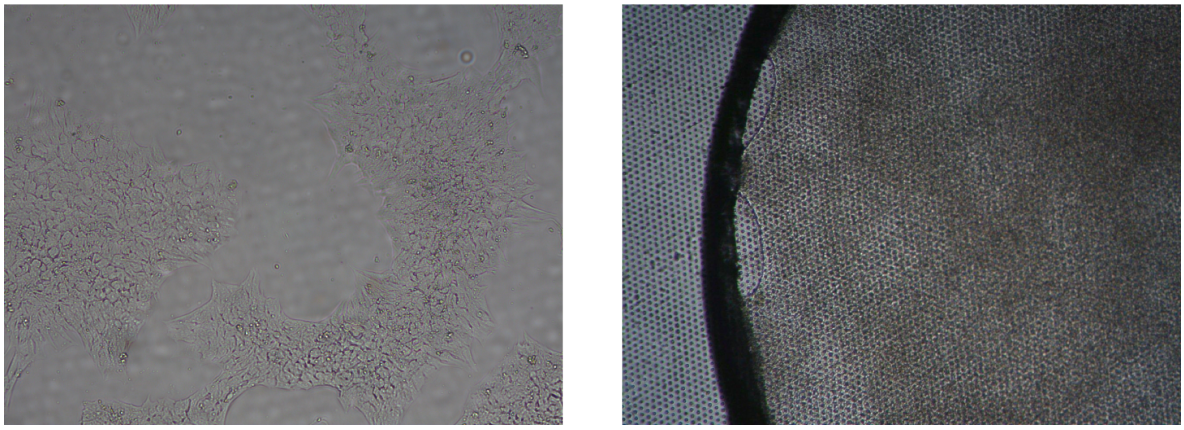

Figure F-2: *Micrographs from inverted bright-field microscope showing seeding and adhesion of MDA-MB-231 breast cancer cells as a 2D cell monolayer on the fribonectin coated PDMS membranes. (left) Poor confluence of the cells at early stage of cell culture. (right) Large confluence of the cells on the membrane.*

Cell Migratrion

By analyzing the cell culture substrate with a bright field microscope, it is possible to locate the cells on either side of the membrane by adjusting the focus. Cells were seen to migrate in the gel while maintaining a round morphology. The brightfield micrographs were manipulated with ImageJ to enhance visibility of cells. The procedure done was to set the threshold to an appropriate level and then using the 'Process / Find Edges' function.

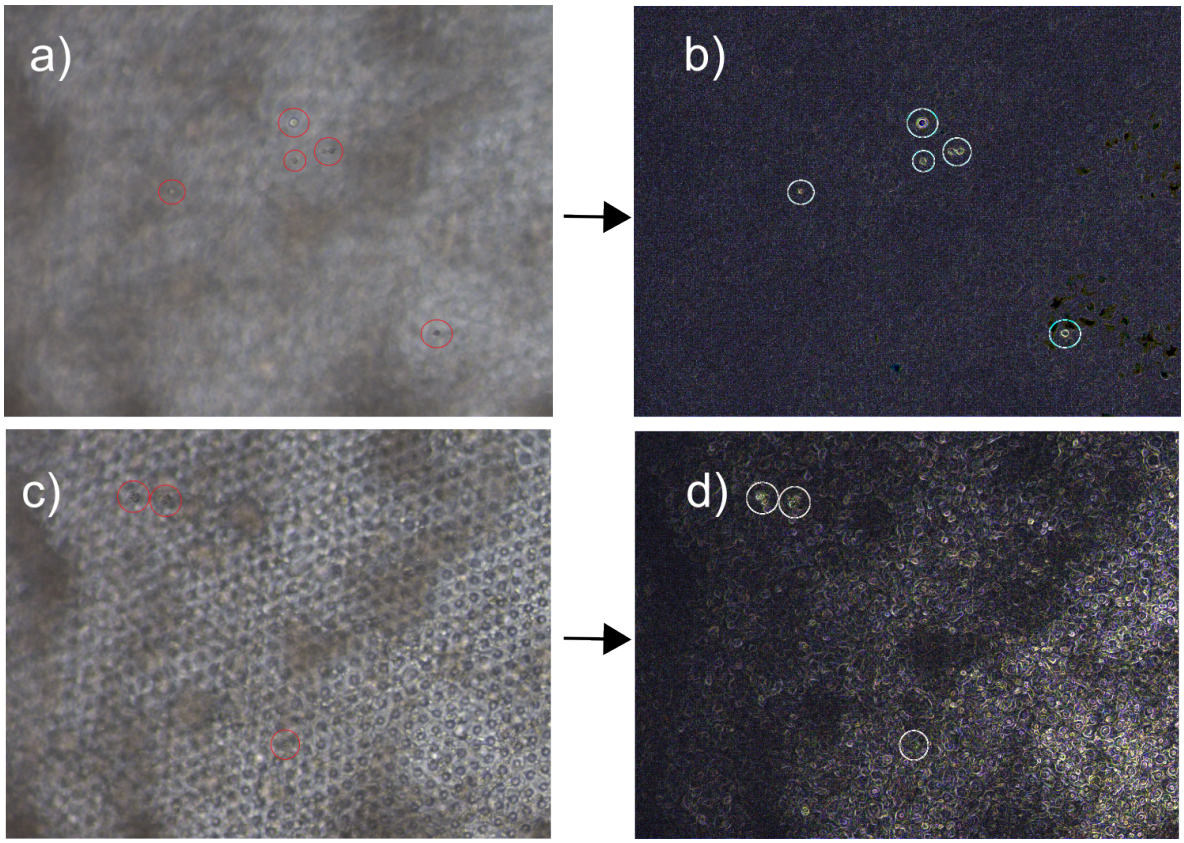

Figure F-3: *(a&c) Brightfield micrographs of observed cell migration through the porous membrane. (b&d) Manipulated images for easier visualization of migrating cells. The method is observed to be more efficient for cells further away at a different focal plane from the porous membrane, compare (b) to (c).*

Bibliography

[1] C. Y. Chan, P.-H. Huang, F. Guo, X. Ding, V. Kapur, J. D. Mai, P. K. Yuen, and T. J. Huang, "Accelerating drug discovery via organs-on-chips," *Lab on a chip*, vol. 13, no. 24, pp. 4697–4710, 2013.

[2] D. Huh, B. D. Matthews, A. Mammoto, M. Montoya-Zavala, H. Y. Hsin, and D. E. Ingber, "Reconstituting organ-level lung functions on a chip," *Science*, vol. 328, no. 5986, pp. 1662–1668, 2010.

[3] A. van de Stolpe and J. den Toonder, "Workshop meeting report organs-on-chips: human disease models," *Lab on a chip*, vol. 13, no. 18, pp. 3449–3470, 2013.

[4] E. W. Young, "Cells, tissues, and organs on chips: challenges and opportunities for the cancer tumor microenvironment," *Integrative Biology*, vol. 5, no. 9, pp. 1096–1109, 2013.

[5] S. Khoshfetrat Pakazad, A. Savov, A. Van De Stolpe, S. Braam, B. Van Meer, and R. Dekker, "A stretchable micro-electrode array for in vitro electrophysiology," in *Micro Electro Mechanical Systems (MEMS), 2011 IEEE 24th International Conference on*, pp. 829–832, IEEE, 2011.

[6] G. P. Gupta and J. Massagué, "Cancer metastasis: building a framework," *Cell*, vol. 127, no. 4, pp. 679–695, 2006.

[7] D. Wlodkowic and J. M. Cooper, "Tumors on chips: oncology meets microfluidics," *Current opinion in chemical biology*, vol. 14, no. 5, pp. 556–567, 2010.

[8] K. E. Sung, N. Yang, C. Pehlke, P. J. Keely, K. W. Eliceiri, A. Friedl, and D. J. Beebe, "Transition to invasion in breast cancer: a microfluidic in vitro model enables examination of spatial and temporal effects," *Integrative Biology*, vol. 3, no. 4, pp. 439–450, 2011.

[9] P. Carmeliet and R. K. Jain, "Angiogenesis in cancer and other diseases," *Nature*, vol. 407, no. 6801, pp. 249–257, 2000.

[10] J. De Jong, R. Lammertink, and M. Wessling, "Membranes and microfluidics: a review," *Lab on a Chip*, vol. 6, no. 9, pp. 1125–1139, 2006.

[11] B.-h. Chueh, D. Huh, C. R. Kyrtsos, T. Houssin, N. Futai, and S. Takayama, "Leakage-free bonding of porous membranes into layered microfluidic array systems," *Analytical chemistry*, vol. 79, no. 9, pp. 3504–3508, 2007.

[12] E. Berthier, E. W. Young, and D. Beebe, "Engineers are from pdms-land, biologists are from polystyrenia," *Lab on a Chip*, vol. 12, no. 7, pp. 1224–1237, 2012.

[13] R. Mukhopadhyay, "When pdms isn't the best," *Analytical chemistry*, vol. 79, no. 9, pp. 3248–3253, 2007.

[14] D. Huh, H. J. Kim, J. P. Fraser, D. E. Shea, M. Khan, A. Bahinski, G. A. Hamilton, and D. E. Ingber, "Microfabrication of human organs-on-chips," *Nature protocols*, vol. 8, no. 11, pp. 2135–2157, 2013.

[15] W. Chen, R. H. Lam, and J. Fu, "Photolithographic surface micromachining of polydimethylsiloxane (pdms)," *Lab on a Chip*, vol. 12, no. 2, pp. 391–395, 2012.

[16] W. Chen, N.-T. Huang, B. Oh, R. H. Lam, R. Fan, T. T. Cornell, T. P. Shanley, K. Kurabayashi, and J. Fu, "Surface-micromachined microfiltration membranes for efficient isolation and functional immunophenotyping of subpopulations of immune cells," *Advanced healthcare materials*, vol. 2, no. 7, pp. 965–975, 2013.

[17] J. H. Koschwanez, R. H. Carlson, and D. R. Meldrum, "Thin pdms films using long spin times or tert-butyl alcohol as a solvent," *PLoS one*, vol. 4, no. 2, p. e4572, 2009.

[18] H. Wei, B.-h. Chueh, H. Wu, E. W. Hall, C.-w. Li, R. Schirhagl, J.-M. Lin, and R. N. Zare, "Particle sorting using a porous membrane in a microfluidic device," *Lab on a chip*, vol. 11, no. 2, pp. 238–245, 2011.

[19] A. L. Thangawng, R. S. Ruoff, M. A. Swartz, and M. R. Glucksberg, "An ultra-thin pdms membrane as a bio/micro–nano interface: fabrication and characterization," *Biomedical microdevices*, vol. 9, no. 4, pp. 587–595, 2007.

[20] R. J. Jackman, D. C. Duffy, O. Cherniavskaya, and G. M. Whitesides, "Using elastomeric membranes as dry resists and for dry lift-off," *Langmuir*, vol. 15, no. 8, pp. 2973–2984, 1999.

[21] T. Masters, W. Engl, Z. L. Weng, B. Arasi, N. Gauthier, and V. Viasnoff, "Easy fabrication of thin membranes with through holes. application to protein patterning," *PloS one*, vol. 7, no. 8, p. e44261, 2012.

[22] K. H. Lau, A. Giridhar, S. Harikrishnan, N. Satyanarayana, and S. K. Sinha, "Releasing high aspect ratio su-8 microstructures using az photoresist as a sacrificial layer on metallized si substrates," *Microsystem technologies*, vol. 19, no. 11, pp. 1863–1871, 2013.

[23] C. Luo, A. Govindaraju, J. Garra, T. Schneider, R. White, J. Currie, and M. Paranjape, "Releasing su-8 structures using polystyrene as a sacrificial material," *Sensors and Actuators A: Physical*, vol. 114, no. 1, pp. 123–128, 2004.

[24] K. A. Addae-Mensah, R. S. Reiserer, and J. P. Wikswo, "Poly (vinyl alcohol) as a structure release layer for the microfabrication of polymer composite structures," *Journal of Micromechanics and Microengineering*, vol. 17, no. 7, p. N41, 2007.

[25] V. Linder, B. D. Gates, D. Ryan, B. A. Parviz, and G. M. Whitesides, "Water-soluble sacrificial layers for surface micromachining," *Small*, vol. 1, no. 7, pp. 730–736, 2005.

[26] J. J. VanDersarl, A. M. Xu, and N. A. Melosh, "Rapid spatial and temporal controlled signal delivery over large cell culture areas," *Lab on a Chip*, vol. 11, no. 18, pp. 3057–3063, 2011.

[27] H. H. Chung, C. K. Chan, T. S. Khire, G. A. Marsh, A. Clark, R. E. Waugh, and J. L. McGrath, "Highly permeable silicon membranes for shear free chemotaxis and rapid cell labeling," *Lab on a Chip*, 2014.

[28] K. Chaw, M. Manimaran, F. Tay, and S. Swaminathan, "Matrigel coated polydimethylsiloxane based microfluidic devices for studying metastatic and non-metastatic cancer cell invasion and migration," *Biomedical microdevices*, vol. 9, no. 4, pp. 597–602, 2007.

[29] L. S. Corning Inc., "Transwell permeable supports selection and use guide," 2010.

[30] K. Paňková, D. Rösel, M. Novotnỳ, and J. Brábek, "The molecular mechanisms of transition between mesenchymal and amoeboid invasiveness in tumor cells," *Cellular and molecular life sciences*, vol. 67, no. 1, pp. 63–71, 2010.

[31] J. Moresco, C. H. Clausen, and W. Svendsen, "Improved anti-stiction coating of su-8 molds," *Sensors and Actuators B: Chemical*, vol. 145, no. 2, pp. 698–701, 2010.

[32] J. Zhou, A. V. Ellis, and N. H. Voelcker, "Recent developments in pdms surface modification for microfluidic devices," *Electrophoresis*, vol. 31, no. 1, pp. 2–16, 2010.

[33] A. Del Campo and C. Greiner, "Su-8: a photoresist for high-aspect-ratio and 3d submicron lithography," *Journal of Micromechanics and Microengineering*, vol. 17, no. 6, p. R81, 2007.

[34] S. Takayama, E. Ostuni, X. Qian, J. C. McDonald, X. Jiang, P. LeDuc, M.-H. Wu, D. E. Ingber, and G. M. Whitesides, "Topographical micropatterning of poly (dimethylsiloxane) using laminar flows of liquids in capillaries," *Advanced materials*, vol. 13, no. 8, pp. 570–574, 2001.

[35] B. Balakrisnan, S. Patil, and E. Smela, "Patterning pdms using a combination of wet and dry etching," *Journal of Micromechanics and Microengineering*, vol. 19, no. 4, p. 047002, 2009.

[36] A. van de Stolpe, "On the origin and destination of cancer stem cells: a conceptual evaluation," *American journal of cancer research*, vol. 3, no. 1, p. 107, 2013.

[37] D. T. Butcher, T. Alliston, and V. M. Weaver, "A tense situation: forcing tumour progression," *Nature Reviews Cancer*, vol. 9, no. 2, pp. 108–122, 2009.

[38] H. Yu, J. K. Mouw, and V. M. Weaver, "Forcing form and function: biomechanical regulation of tumor evolution," *Trends in cell biology*, vol. 21, no. 1, pp. 47–56, 2011.

[39] S. Kumar and V. M. Weaver, "Mechanics, malignancy, and metastasis: the force journey of a tumor cell," *Cancer and Metastasis Reviews*, vol. 28, no. 1-2, pp. 113–127, 2009.

[40] I. Ramis-Conde, M. A. Chaplain, A. R. Anderson, and D. Drasdo, "Multi-scale modelling of cancer cell intravasation: the role of cadherins in metastasis," *Physical biology*, vol. 6, no. 1, p. 016008, 2009.

[41] J. A. Joyce and J. W. Pollard, "Microenvironmental regulation of metastasis," *Nature Reviews Cancer*, vol. 9, no. 4, pp. 239–252, 2009.

[42] Y.-s. Torisawa, B. Mosadegh, S. P. Cavnar, M. Ho, and S. Takayama, "Transwells with microstamped membranes produce micropatterned two-dimensional and three-dimensional co-cultures," *Tissue Engineering Part C: Methods*, vol. 17, no. 1, pp. 61–67, 2010.

[43] S.-J. Wang, W. Saadi, F. Lin, C. Minh-Canh Nguyen, and N. Li Jeon, "Differential effects of egf gradient profiles on mda-mb-231 breast cancer cell chemotaxis," *Experimental cell research*, vol. 300, no. 1, pp. 180–189, 2004.

[44] J. W. Song, S. P. Cavnar, A. C. Walker, K. E. Luker, M. Gupta, Y.-C. Tung, G. D. Luker, and S. Takayama, "Microfluidic endothelium for studying the intravascular adhesion of metastatic breast cancer cells," *PloS one*, vol. 4, no. 6, p. e5756, 2009.

[45] S. Even-Ram and K. M. Yamada, "Cell migration in 3d matrix," *Current opinion in cell biology*, vol. 17, no. 5, pp. 524–532, 2005.

[46] B. J. Kim and M. Wu, "Microfluidics for mammalian cell chemotaxis," *Annals of biomedical engineering*, vol. 40, no. 6, pp. 1316–1327, 2012.

[47] K.-J. Jang and K.-Y. Suh, "A multi-layer microfluidic device for efficient culture and analysis of renal tubular cells," *Lab on a Chip*, vol. 10, no. 1, pp. 36–42, 2010.

[48] S. Chung, R. Sudo, P. J. Mack, C.-R. Wan, V. Vickerman, and R. D. Kamm, "Cell migration into scaffolds under co-culture conditions in a microfluidic platform," *Lab on a Chip*, vol. 9, no. 2, pp. 269–275, 2009.

[49] E. T. Roussos, J. S. Condeelis, and A. Patsialou, "Chemotaxis in cancer," *Nature Reviews Cancer*, vol. 11, no. 8, pp. 573–587, 2011.

[50] I. K. Zervantonakis, S. K. Hughes-Alford, J. L. Charest, J. S. Condeelis, F. B. Gertler, and R. D. Kamm, "Three-dimensional microfluidic model for tumor cell intravasation and endothelial barrier function," *Proceedings of the National Academy of Sciences*, vol. 109, no. 34, pp. 13515–13520, 2012.

[51] T. Liu, C. Li, H. Li, S. Zeng, J. Qin, and B. Lin, "A microfluidic device for characterizing the invasion of cancer cells in 3-d matrix," *Electrophoresis*, vol. 30, no. 24, pp. 4285–4291, 2009.